Computers and Structures 305 (2024) 107547

Contents lists available at ScienceDirect

Computers and Structures

journal homepage: www.elsevier.com/locate/compstruc

Control of geometry and stability of tensegrities in the Octahedron and X-Octahedron families

J.F. Carbonell-Márquez [a,*], M.A. Fernández-Ruiz [a], E. Hernández-Montes [b], L.M. Gil-Martín [b]

[a] Departamento de Ingeniería Civil, de Materiales y Fabricación, Universidad de Málaga. C/ Dr. Ortiz Ramos, s/n, 29071 Málaga, Spain
[b] Department of Structural Mechanics, University of Granada (UGR), Campus Universitario de Fuentenueva s/n. 18072 Granada, Spain

ARTICLE INFO

Keywords:
Tensegrity geometry
Tensegrity
Analytical form-finding
Force Density Method
Stability

ABSTRACT

Tensegrity structures obtained from the same connectivity patterns are said to belong to families. The Octahedron and X-Octahedron families are examples of these. In the literature, little attention has been paid to how the final geometries of the equilibrium forms of the members of both families are obtained. A compact formulation for controlling the equilibrium shapes of members of the Octahedron and X-Octahedron families is proposed in this article allowing the designer to get any geometry for the super-stable members of both families. Controlling the stability of folded forms is achieved by using the shape of the structure, and a detailed explanation of the formulation is provided here, as well as several examples that clarify the formulation. The geometrical control of the equilibrium shape is fundamental when applying it to tensegrity structures in an engineering context.

1. Introduction

Tensegrity structures are kinds of structures made up of pin-jointed self-stressed elements, which are tensioned cables and compressed bars, also referred to interchangeably as struts in this work. The purist form of this structure only has one compressed element at each of their nodes [1]. Initially thought of as sculptures, nowadays, tensegrity structures have a wide range of technical uses in many different fields: biomechanics [2,3], robotics [4–6], aerospace [7–9], civil engineering [10–13], new *meta*-materials [14–16], etc.

One of the key aspects in the design of a tensegrity is the sought of the equilibrium shape of the structure, in other words, the form-finding process. There are a vast number of form-finding processes in the literature and one of the main used methods is the Force Density Method (FDM), first introduced by Linkwitz and Schek [17,18]. This method, although originally employed for tension-only structures [19–21] and used for the design of compression-only structures [22–25], has been widely employed for performing the form-finding of tensegrity structures [26–30]. The method linearizes the equilibrium equations of a structure by introducing the force:length ratios or force densities, q, defined as the ratio between the axial force and the length of each member ($q > 0$ for cables and $q < 0$ for struts). Therefore, by assigning different sets of force:length ratios, different equilibrium configurations are obtained.

In this work, a procedure based on the FDM is employed to seek for valid sets of force:length ratios that lead to equilibrium configurations of the structure. The main input to the procedure is the connectivity of the nodes that compose the structure and the type of elements (tensioned cables or compressed bars) that join them. The connectivity can be inferred from intuition based on geometric bodies [29,31] or by considering topological relationships [32,33]. By looking at these relationships, tensegrity families are a great source of tensegrity structures. A tensegrity family is defined as a group of tensegrity structures that share a common connectivity pattern or topology [34–37]. In the previously cited works, the Octahedron, and the X-Octahedron families are presented. As will be explained below, the connectivity patterns of the Octahedron and X-Octahedron family members are based on connection graphs in which there are three basic cell rows.

Given the characteristics of tensegrities structures (self-stressed and no fixed points), it is necessary to impose additional conditions to the equilibrium when seeking for a valid set of force:length ratios. One of the main conditions is the global stability of the structure. The stability condition implies that the structure returns to its original shape after the release of a small, enforced deformation [37,38]. As defined by [39] super-stability is a more robust criterion by which a tensegrity results stable regardless of its material properties and its pre-stress level. In [40]

* Corresponding author.
E-mail addresses: jfcarbonell@uma.es (J.F. Carbonell-Márquez), mafernandez@uma.es (M.A. Fernández-Ruiz), emontes@ugr.es (E. Hernández-Montes), mlgil@ugr.es (L.M. Gil-Martín).

https://doi.org/10.1016/j.compstruc.2024.107547
Received 24 May 2024; Accepted 13 September 2024
Available online 18 September 2024

a study has been carried out on the influence of the different connectivity between the three rows of basic cells (called connectivity levels) on the stability of the members of the Octahedron and X-Octahedron families.

Another important condition to be imposed is related to the concept of full and folded forms, first introduced in [41]. Full forms are tensegrities in which no overlapped nodes exist. In contrast, folded forms are tensegrity structures in which nodes that share the same position in the space exist. Each tensegrity member has a position within the family which means that all the previous members in the family are folded forms obtained from its connectivity pattern [36]. As it will be explained below, the force:length ratios assignation will be fundamental to get a full or folded tensegrity structure.

Previously published works [34,36,37,40] have demonstrated the cubical arrangement of the nodes of the tensegrities belonging to the Octahedron and X-Octahedron families. This characteristic suggests promising engineering applications for these structures, such as tensegrity modules for the construction of temporary structures [13,42] or pedestrian bridges [43]. However, while the form-finding procedure described in the referred works provides a valid set of force:length ratios for the members of the Octahedron and X-Octahedron families, this assignment does not result in a unique final geometric configuration of the structure. Instead, the form-finding method yields a set of vectors that, when linearly combined, determine the nodal coordinates of the structure; however, it is necessary to know in advance the coefficients of the linear combination that provide a specific geometry, or to follow a tedious process of trial and error to achieve the desired configuration. Therefore, a well-defined procedure for achieving the desired geometry of the tensegrity structure is necessary to fully harness the potential engineering applications these structures could offer. Additionally, it has been observed in [40] that determining the geometry of the equilibrium shape in folded forms significantly influences the stability of the resulting tensegrity, whereas this effect on stability has not been observed in super-stable tensegrities [40]. This demonstrates that determination of geometry involves crucial aspects (structural stability) that go far beyond mere aesthetic considerations. As the relationship between structural stability and geometry in the Octahedron and X-Octahedron families has never been addressed in the literature, it warrants further investigation.

Considering these observations, the present work aims to address the identified needs by providing a comprehensive solution for determining the geometry of tensegrity structures within the Octahedron and X-Octahedron families. This study introduces a well-defined analytical procedure that ensures a unique final geometric configuration, enabling the designer to control both the structural shape and dimensions while also considering structural stability. The proposed methodology takes advantage of the fact that the struts in the structure can be grouped into three sets of parallel members with equal length, providing the necessary parameters for the linear combination of the vectors obtained from the form-finding method to achieve the desired geometric configuration of the structure. This feature facilitates the attainment of any super-stable geometry in the case of full forms and allows for the control of stability in the case of folded forms for tensegrities within these families. By managing the geometry of the members in these tensegrity structures, modular construction through the assembly of these elements becomes feasible. This precise control over geometric parameters not only enables the design and fabrication of modular components that can be efficiently assembled into larger constructs but also opens up new possibilities for innovative construction methods. Such an approach leverages the unique properties of tensegrity in modular systems, thereby expanding their potential engineering applications.

As this work is intended to be self-contained, Section 2 reviews the main concepts of FDM as an approach that can be used to perform the analytical form-finding of tensegrity structures and the effects of some parameters in the final structural stability. Section 3 presents the characteristics of the topology of the tensegrity families considered, which are the Octahedron and the X-Octahedron families. A new algorithm is also presented that can be used to obtain connectivity between the nodes belonging to the members of both families. The compact method for controlling the tensegrity structure geometry is detailed in Section 4. Section 5 discusses whether folded tensegrities can be super-stable and how geometry affects the stability of these folded tensegrity forms. Finally, Section 6 contains the main conclusions of the work.

2. Analytical form-finding method for tensegrity structures and stability considerations

The form-finding method for tensegrity structures employed in this study [41] is based on the FDM [17,18], which is generally used for pin-jointed networks. The method solves the equilibrium between the internal forces of the network and the external loads, firstly assuming that the elements in the network (cables and bars) are perfectly rigid, and secondly, introducing the ratio between the force and the length of the cables and bars that the structure is composed of as an input. This second aspect allows a set of linear equations to be obtained. However, in the case of tensegrity structures, form-finding is performed by assuming that there are no external loads and no fixed points, meaning that the internal forces in the element constitute a unique state of pre-stress.

Once the connectivity of the n nodes by m branches is defined according to the topology of the family they belong to, the $\mathbf{C} \in \mathbb{R}^{m\times n}$ connectivity matrix is built so that if the k member connects the i and j ($i < j$) nodes then the i-th and the j-th elements of the k-th row of $\mathbf{C}$ are set to 1 and -1 respectively, as presented in Eq. (1):

$$C_{kr} = \begin{cases} 1 & \text{if } i(k) = r \\ -1 & \text{if } j(k) = r \\ 0 & \text{in other cases} \end{cases} \tag{1}$$

with r denoting the r-th column of the k-th row in the $\mathbf{C}$ matrix.

As there are no fixed nodes when dealing with the form-finding of tensegrity structures, equilibrium means solving the set of homogeneous equations presented in Eq. (2):

$$\begin{aligned} \mathbf{D}\cdot\mathbf{x} &= 0 \\ \mathbf{D}\cdot\mathbf{y} &= 0 \\ \mathbf{D}\cdot\mathbf{z} &= 0 \end{aligned} \tag{2}$$

with $\mathbf{D} = \mathbf{C}^{\mathrm{T}}\cdot\mathbf{Q}\cdot\mathbf{C}(\in \mathbb{R}^{n\times n})$ as the force density matrix, $\mathbf{x}$, $\mathbf{y}$, and $\mathbf{z}$ ($\in \mathbb{R}^{n}$) are the nodal coordinate vectors and $\mathbf{Q}$ ($\in \mathbb{R}^{m\times m}$) is the diagonal square matrix of vector $\mathbf{q}$ ($\in \mathbb{R}^{m}$) that contains the force:length ratio q_i of the branch i in its i −th element, $\mathbf{Q} = \mathrm{diag}(\mathbf{q})$. The symbol $^{\mathrm{T}}$ represents the transpose operation of a matrix or vector. The $\mathbf{D}$ matrix can be directly written as:

$$D_{ij} = \begin{cases} \sum_{k\in\Gamma_i} q_k & \text{for } i = j \\ -q_k & \text{if } i \text{and } j \text{linked by } k \\ 0 & \text{for the rest} \end{cases} \tag{3}$$

with Γ_i the set of elements having i as a node.

Tensegrities can be obtained in three different dimensions. If d indicates the dimension in which the tensegrity structure is developed, when $d = 1$ a tensegrity structure is obtained where all its nodes lie on a line. If $d = 2$, all the nodes of the tensegrity structure are on the same plane. Finally, if $d = 3$, then a 3D tensegrity structure is obtained, and its nodes occupy different positions in space, creating a volume within them. As presented by [41] and [37], the non-degeneracy condition must be fulfilled so that the rank deficiency of $\mathbf{D}$ has to be at least $d+1 = 4$ in order to get a 3D tensegrity structure ($d = 3$). According to [1], if a structure lies in a d-dimensional space with smaller dimension than d (i.e. a plane structure, $d = 2$, presented in 3D) then the structure is considered degenerate in such space; on the contrary, the structure is said to be non-degenerate. As Eq. (3) defines $\mathbf{D}$ as a symmetrical real matrix, it is orthogonally diagonalizable by the spectral theorem.

Therefore, the non-degeneracy condition means 0 has a multiplicity of at least 4 as an eigenvalue of **D**. Let be $\lambda = \mathbf{P}^{-1}\cdot\mathbf{D}\cdot\mathbf{P}$ ($\in \mathbb{R}^{m\times m}$) a diagonal matrix that contains the eigenvalues of the **D** matrix and **P** an orthogonal matrix whose columns correspond to an orthonormal base of eigenvectors of **D**. If the non-degeneracy condition is to be fulfilled, then the dimension of the null space of the **D** matrix, ker**D**, must also be at least 4.

If $p(\lambda) = \lambda^n + a_{n-1}\lambda^{n-1} + \cdots + a_1\lambda + a_0$ is the characteristic polynomial of **D**, then the a_i coefficients can be written as a function of the force: length ratios assigned to the structure: $a_i = a_i(q_1, q_2, \cdots q_m) = a_i(\mathbf{q})$. As, by construction of **D**, the sum of all components in each row or column is zero, Eq. (3), then $a_0 = |\mathbf{D}| = 0$, and the necessary condition for finding a 3D tensegrity is:

$$a_i(\mathbf{q}) = 0, \text{with } i = 1, 2, 3. \tag{4}$$

This last condition given in Eq. (4) constitutes a set of polynomial equations in **q** that can be analytically solved. The complexity of Eq. (4) can be reduced if some relations between the force:length ratios of the members of the tensegrity are imposed. When a set of q values (or a **q** vector) that satisfies Eq. (4) is found, the **D** matrix that corresponds to those values can be constructed, and solutions for **x**, **y**, and **z** that satisfy equilibrium, Eq. (2), can be calculated. By definition, the vectors of nodal coordinates **x**, **y**, and **z** belong to the null space of the **D** matrix meaning that if the base of this subspace is composed of $\mathbf{e}^i \in \mathbb{R}^n$ ($i = \mathrm{I}, \mathrm{II}, \cdots, \mathrm{Y}$), with Y as the roman counterpart of $\upsilon = \dim(\ker[\![\mathbf{D}]\!])$, then the coordinates of the tensegrity nodes can be expressed as a linear combination of $\mathbf{e}^i$:

$$\begin{aligned}\mathbf{x} &= \sum_{i=\mathrm{I}}^{\mathrm{Y}} \alpha_x^i \mathbf{e}^i \\ \mathbf{y} &= \sum_{i=\mathrm{I}}^{\mathrm{Y}} \alpha_y^i \mathbf{e}^i \\ \mathbf{z} &= \sum_{i=\mathrm{I}}^{\mathrm{Y}} \alpha_z^i \mathbf{e}^i\end{aligned} \tag{5}$$

which can be written in matrix form as:

$$\mathbf{X} = (\mathbf{x} \quad \mathbf{y} \quad \mathbf{z}) = \left(\mathbf{e}^{\mathrm{I}} \quad \mathbf{e}^{\mathrm{II}} \quad \cdots \quad \mathbf{e}^{\mathrm{Y}}\right) \underbrace{\begin{pmatrix} \alpha_x^{\mathrm{I}} & \alpha_y^{\mathrm{I}} & \alpha_z^{\mathrm{I}} \\ \alpha_x^{\mathrm{II}} & \alpha_y^{\mathrm{II}} & \alpha_z^{\mathrm{II}} \\ \vdots & \vdots & \vdots \\ \alpha_x^{\mathrm{Y}} & \alpha_y^{\mathrm{Y}} & \alpha_z^{\mathrm{Y}} \end{pmatrix}}_{\alpha} \tag{6}$$

where α_j^i with $j = x, y, z$ and $i = \mathrm{I}, \mathrm{II}, \cdots, \mathrm{Y}$ are arbitrary real numbers. The $\mathbf{e}^i$ vectors that compose the base of ker**D** are the linear independent eigenvectors of **D** that correspond to 0 with υ multiplicity. Eq. (5) shows that $\mathbf{e}^i$ vectors constitute the base of the space of equilibrium solutions for a given force:length ratio value and for a particular topology or connectivity between the nodes of the structure. The minimum dimension of ker**D** required for a 3D non-degenerate tensegrity is 4, and the ker**D** = 4 condition needs be satisfied to obtain [39] super-stable tensegrities [1,34,35,37,40]. Therefore, $\upsilon = 4$ and Y = IV are going to be considered in the subsequent mathematical developments.

Note that the non-degeneracy condition regarding the rank deficiency of the **D** matrix for a 3D structure is a necessary but not sufficient condition. As well as this, the linear independence of the coordinate vectors should also be satisfied for a 3D structure [1]. This is achieved when matrix $\alpha \in \mathbb{R}^{4\times 3}$ in Eq. (6) has full rank (i.e. $rank(\alpha) = 3$).

For each value of **q** that satisfies Eq. (4), the stability of the tensegrity is checked. The stability of a tensegrity means that it returns to its original shape (equilibrium configuration) after release of a small, enforced deformation [37]. It has been stated that a 3D ($d = 3$) tensegrity is super-stable if it is always stable, regardless of its material properties and pre-stress levels, and it means that the following three conditions [1,38,39] need to be satisfied:

1. The rank deficiency of the **D** force density matrix is exactly $d + 1 = 4$
2. **D** is positive semi-definite (i.e., $\lambda_i \geq 0$)
3. The rank of the geometry matrix **G** is $\frac{d^2+d}{2} = 6$

with the geometry matrix $\mathbf{G} = (\mathbf{U}\cdot\mathbf{u}, \mathbf{V}\cdot\mathbf{v}, \mathbf{W}\cdot\mathbf{w}, \mathbf{U}\cdot\mathbf{v}, \mathbf{U}\cdot\mathbf{w}, \mathbf{V}\cdot\mathbf{w}) \in \mathbb{R}^{m\times\frac{d^2+d}{2}}$, $\mathbf{u} = \mathbf{C}\cdot\mathbf{x}, \mathbf{v} = \mathbf{C}\cdot\mathbf{y}, \mathbf{w} = \mathbf{C}\cdot\mathbf{z}, \mathbf{U} = \mathrm{diag}(\mathbf{u}), \mathbf{V} = \mathrm{diag}(\mathbf{v}), \mathbf{W} = \mathrm{diag}(\mathbf{w})$. A less robust criterion than super-stability is just stability. A structure is stable if all the eigenvalues of the structure tangent stiffness matrix, **K** matrix, if the $\left([\![d]\!]^2 + d\right)/2 = 6$ zero eigenvalues corresponding to 3D rigid-body motions are not considered, as explained by [1]. Further insights on tensegrity structures stability can be found in [1,37,39].

3. The Octahedron and X-Octahedron tensegrity families

The present work is focused on the Octahedron [34,37] and X-Octahedron [36] families whose general topological patterns have been recently proposed in the literature [40]. All the members of the Octahedron and X-Octahedron families are composed of rhombic and X-rhombic cells, respectively (see Fig. 1).

Fig. 1(a) shows that the rhombic cells in the Octahedron family consists of 4 nodes connected by cables (or tensile elements), and only two of them are linked by a strut (or compressed bar). Nodes that are not connected by the strut are the principal nodes of the cell, while the others are the secondary ones. The basic cell of the X-Octahedron family, Fig. 1(b), is the same, except for an additional cable linking the two principal nodes in the cell.

In the present work, the p parameter will be employed to establish the position of a particular tensegrity structure in the family. The first members ($p = 1$) in the Octahedron and the X-Octahedron families are the octahedron and the X-octahedron, which consist of 6 nodes connected by 3 struts and 12 or 15 cables, respectively. All the members ($p > 1$) of both families are built from the expansion of the first members, whose connectivity are presented in Fig. 2.

As explained in [37], the expansion of the different members of both families is produced in such a way that each node, cable, and strut in a member of the family is duplicated in the subsequent one. Therefore, the number of nodes in the p-th member is $n = 3\cdot 2^p$, the number of struts or compressed bars is $n_b = 3\cdot 2^{p-1}$, and the number of cables is $n_c = 3\cdot 2^{p+1}$ ($m = n_c + n_b = 15\cdot 2^{p-1}$) or $n_c = 15\cdot 2^{p-1}$ ($m = n_c + n_b = 18\cdot 2^{p-1}$) depending on whether the tensegrity belongs to the Octahedron or X-Octahedron family, respectively. Fig. 3 shows some members of both families together with their numbers of nodes, cables, and struts.

To take the nodal connectivity for members beyond the octahedron or the X-octahedron ($p > 1$) to define matrix **C**, the plane connection graph, which is a graphical representation of the connectivity between the nodes of the tensegrity, needs to be constructed. The plane connection graph is made by drawing a $3 \times 2^{p-1}$ matrix of basic cellular cells meaning that the numeration of each node is given by the position of the basic cell within the matrix, as the algorithm presented in Fig. 4 indicates. The row occupied by a particular cell is provided by the $k \in [1, 3]$ parameter. The 2^{p-1} columns are constructed in pairs so that the $i \in [1, 2^{p-2}]$ parameter controls the pair, and the $j \in [1, 2]$ parameter gives the cell within the pair. Therefore, for a given cell corresponding to the triad $(k.i,j)$, the numeration of its four nodes is, Fig. 4:

$$\begin{aligned} a &= j + 4\cdot(i-1) + 2^p\cdot(k-1) \\ b &= (j+2) + 4\cdot(i-1) + 2^p\cdot(k-1) \\ c &= j + 2\cdot(i-1) + 2^p\cdot[(k-1)+_3 2] \\ d &= (3-j) + 2\cdot(i-1) + 2^p\cdot[(k-1)+_3 2] + 2^{p-1} \end{aligned} \tag{7}$$

where $[(k-1)+_3 2] = [(k-1)+2] mod 3$ and $p > 1$.

As an example, the plane connection graphs for the double-expanded octahedron and the X-double-expanded octahedron ($p = 3$) are pro-

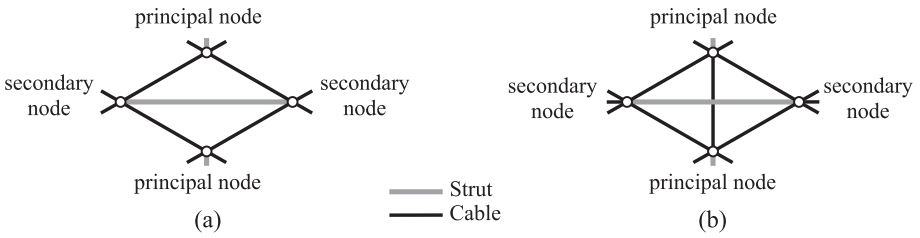

Fig. 1. Basic rhombic cells employed in (a) Octahedron and (b) X-Octahedron families.

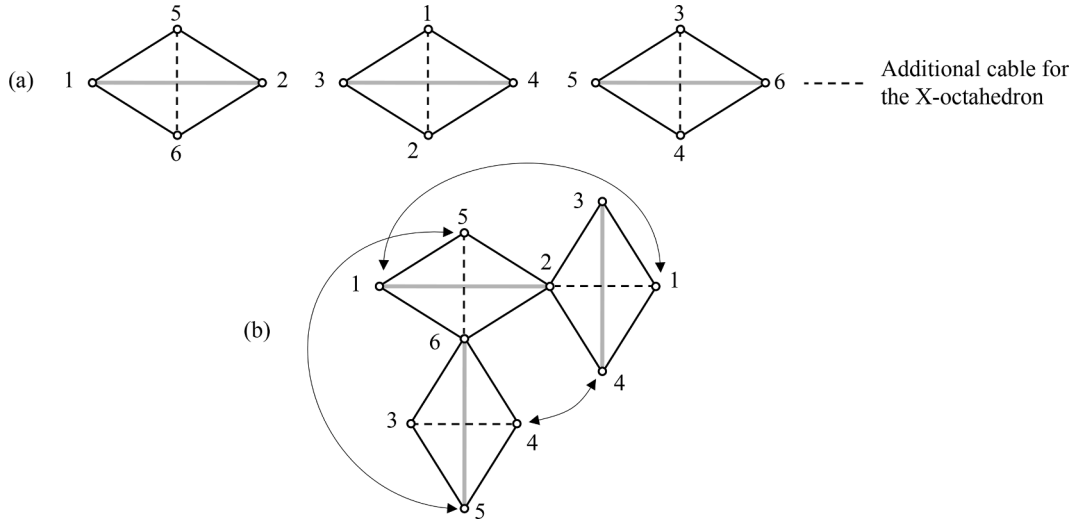

Fig. 2. (a) Plane connection graph for the octahedron ($p = 1$). The dashed lines indicate the additional cable necessary to get the plane connection graph for the X-octahedron. The three basic cells are connected so that nodes with the same numbering match (b). The curved lines in (b) indicate how the same nodes have to be connected.

vided in Fig. 5. In this case, $i \in \left[1, 2^{p-2}\right] = [1, 2]$.

Once the connectivity graph is constructed and the **C** matrix is obtained, the next important aspect that requires attention is the assignment of force:length ratios to cables and struts. It has already been mentioned that the q values adopted are important if the non-degeneracy condition of the structure, i.e., to obtain a fully developed tensegrity in 3D, is to be met. However, even if that condition is fulfilled, the assignation of some sets of q values could lead to a 3D structure in which some nodes, cables, and struts share the same position in the space, i.e., overlap. These equilibrium configurations are called folded forms [41], as opposed to full forms which are tensegrity structures whose nodes adopt different positions in space. A unique feature of tensegrity families is that the p-th member of the family is a folded form of all the subsequent members of the family.

According to [34], if only two values of force:length ratios are considered (q_c for cables and q_b for struts), the full super-stable form of the p-th member of the Octahedron family is obtained if the assigned force:length ratios create the following relation:

$$\frac{q_b}{q_c} = -\frac{p+1}{p} \tag{8}$$

Similarly, the full super-stable form of the p-th member of the X-Octahedron family is obtained if the ratio $\frac{q_b}{q_c}$ fulfills the following condition, as presented in [40]:

$$\frac{q_b}{q_c} = -\frac{2p+1}{2p-1} \tag{9}$$

If the $\frac{q_b}{q_c}$ ratios presented in Eqs. (8) and (9) are known, the analytical resolution of the set of polynomial equations in **q** given by Eq. (4) is no longer necessary, leading to significant computational savings. For example, in the case of the X-double-expanded octahedron ($p = 3$), the solutions provided by Eq. (4) are $\frac{q_b}{q_c} = -\frac{7}{5}$, $\frac{q_b}{q_c} = -\frac{5}{3}$, $\frac{q_b}{q_c} = -3$ [36]. These solutions are the same as those obtained from Eq. (9) for $p = 3$, $p = 2$, and $p = 1$, respectively. The first solution corresponds to the full form, while the other two are folded forms (X-expanded octahedron and X-octahedron, respectively).

4. Controlling the geometry of the Octahedron and x-octahedron tensegrity families

4.1. Mathematical development

As stated earlier, Eq. (5), the nodal coordinates of a tensegrity structure (which are placed at vectors **x**, **y**, and **z**) are calculated as linear combinations of the vectors of the basis of ker**D**, $\mathbf{e}^i$, with $i = \mathrm{I}, \cdots, \mathrm{VI}$. The $\mathbf{e}^i$ vectors are the eigenvectors that correspond to four zero eigenvalues of the **D** matrix. As proved in [1], if the tensegrity structure is non-degenerate in the 3-dimensional space, then its nodal coordinate

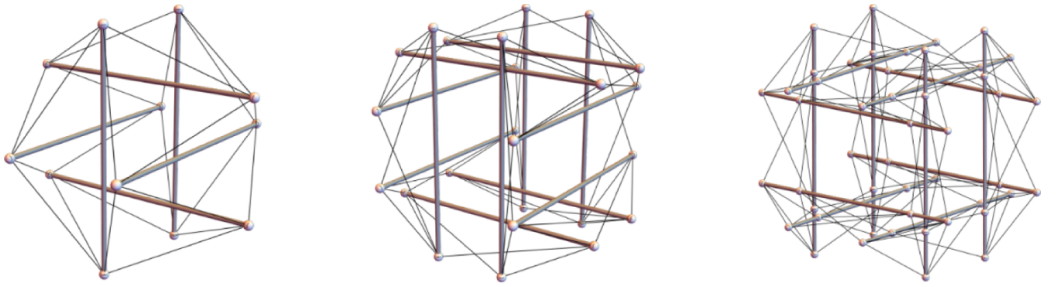

Expanded octahedron (p =2) | Double-expanded octahedron (p =3) | Triple-expanded octahedron (p =4)

Nodes (n): 12 | Nodes (n): 24 | Nodes (n): 48
Cables (n_c): 24 | Cables (n_c): 48 | Cables (n_c): 96
Struts (n_s): 6 | Struts (n_s): 12 | Struts (n_s): 24

(a) Octahedron family

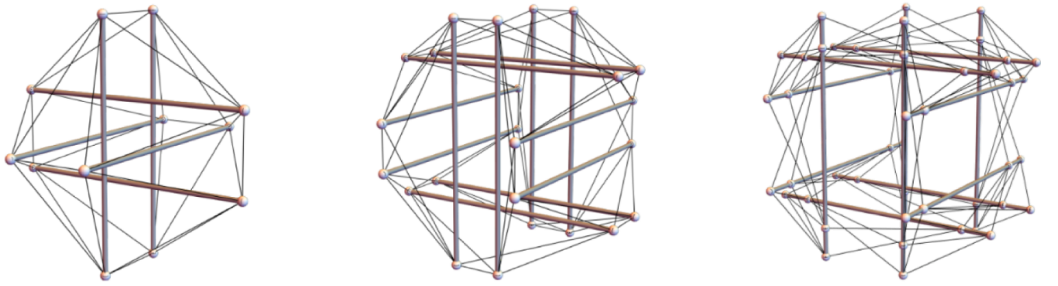

X-expanded octahedron (p =2) | X-double-expanded octahedron (p =3) | Triple-expanded octahedron (p =4)

Nodes (n): 12 | Nodes (n): 24 | Nodes (n): 48
Cables (n_c): 30 | Cables (n_c): 60 | Cables (n_c): 120
Struts (n_s): 6 | Struts (n_s): 12 | Struts (n_s): 24

(b) X- Octahedron family

Fig. 3. Second, third, and fourth members of the (a) Octahedron and (b) X-Octahedron families.

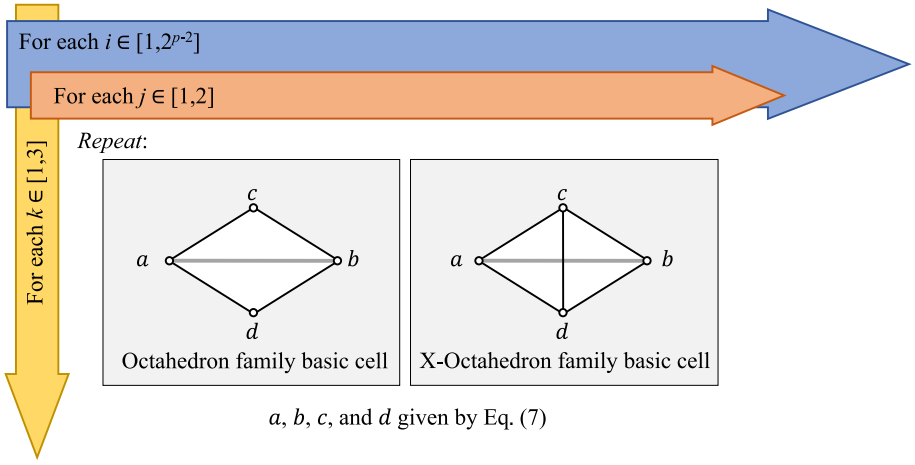

Fig. 4. Algorithm for the construction of the plane connection graph.

vectors in each direction of space are linearly independent, i.e., the α matrix in Eq. (6) needs to have full rank. Different matrices α lead to different geometries of the tensegrity structure in space, Fig. 6, as the linear combination of the vectors of the basis of ker**D** changes.

When obtaining the geometry of the different members of the Octahedron and X-Octahedron families, one important aspect is that there are always three groups of struts that are parallel and have the same length no matter which linear combination of vectors of the basis of ker**D** is selected. Fig. 6 also shows this. As the octahedron and the X-octahedron ($p = 1$) have three struts, the expanded and the X-expanded octahedron ($p = 2$) have three groups of two equal and parallel compressed bars. The double-expanded and the X-double-expanded octahedron ($p = 3$) have the same three groups, but each of them is composed of 4 parallel equal struts. Therefore, the p −th member has three groups of 2^{p-1} equal and parallel compressed bars. These three groups of struts correspond to each of the three rows of paired rhombic

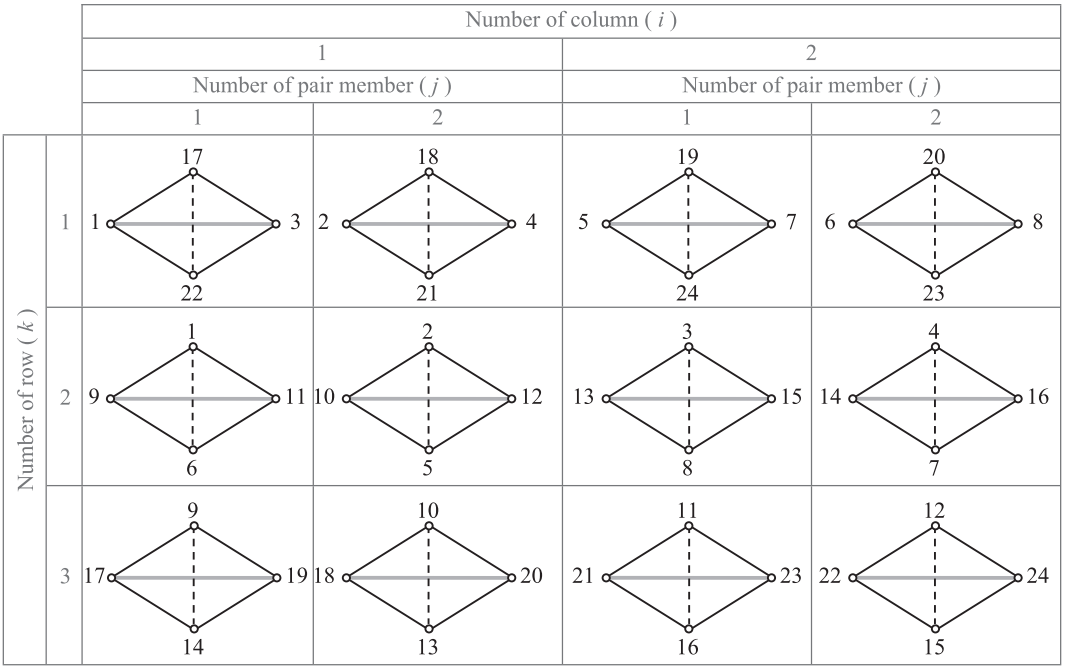

Fig. 5. Plane connection graph for the double-expanded and X-double-expanded octahedron ($p = 3$). The dashed lines indicate the additional cable needed for the plane connection graph for the X-double-expanded-octahedron.

$$\text{Basis of } \ker \mathbf{D} = \begin{cases} \mathbf{e}^{\mathrm{I}} = (7 \quad -3 \quad -1 \quad 5 \quad 4 \quad 0 \quad 4 \quad 0 \quad 4 \quad 0 \quad 0 \quad 4)^{\mathrm{T}} \\ \mathbf{e}^{\mathrm{II}} = (7 \quad -77 \quad -149 \quad 79 \quad 78 \quad -148 \quad -70 \quad 0 \quad -70 \quad 0 \quad 74 \quad -144)^{\mathrm{T}} \\ \mathbf{e}^{\mathrm{III}} = (-7 \quad 77 \quad -3 \quad 73 \quad -2 \quad 72 \quad 70 \quad 0 \quad -63 \quad 133 \quad 97 \quad -27)^{\mathrm{T}} \\ \mathbf{e}^{\mathrm{IV}} = (-1 \quad 11 \quad 11 \quad -1 \quad 14 \quad -4 \quad -10 \quad 20 \quad 11 \quad -1 \quad 11 \quad -1)^{\mathrm{T}} \end{cases}$$

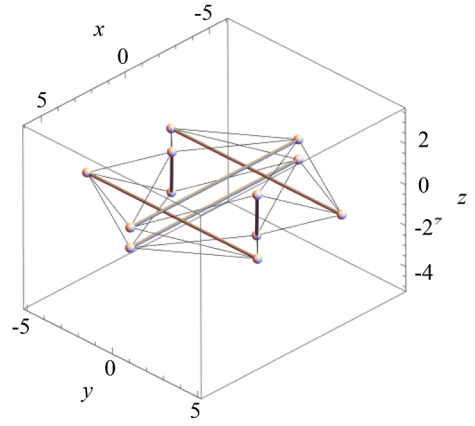

$$\boldsymbol{\alpha} = \begin{pmatrix} -793{,}92 & -13{,}41 & 14{,}10 & 125{,}00 \\ -118{,}24 & -12{,}40 & 30{,}07 & -250{,}00 \\ -167{,}22 & 9{,}05 & 18{,}61 & 0{,}00 \end{pmatrix}^{\mathrm{T}} \cdot 10^{-3}$$

(a)

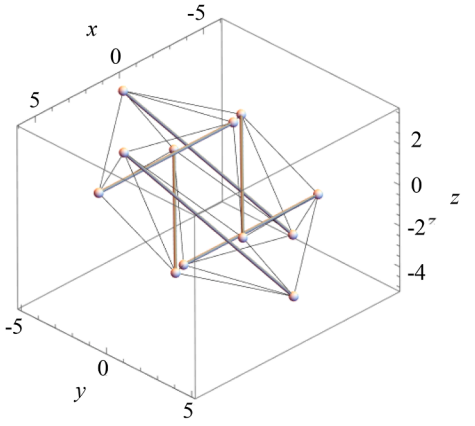

$$\boldsymbol{\alpha} = \begin{pmatrix} -709{,}46 & -20{,}00 & 32{,}51 & -76{,}78 \\ 168{,}92 & -22{,}44 & -6{,}83 & -176{,}78 \\ -238{,}89 & 12{,}93 & 26{,}58 & 0{,}00 \end{pmatrix}^{\mathrm{T}} \cdot 10^{-3}$$

(b)

Fig. 6. Two different 3D realizations of the expanded octahedron ($p = 2$) from two different matrices α. The basis of ker$\boldsymbol{D}$ is indicated in the figure as well as the different matrices α to get the tensegrities (a) and (b).

cells on the plane connection graph (controlled by the k parameter in Fig. 4).

Let the director member of group k ($k = 1,2,3$) of struts be defined as the bar that links the r_k and s_k ($r_k > s_k$) nodes with lowest indices in the group of struts (i.e., $i = j = 1$ in Eq. (7)). According to Eq. (7) and the algorithm of connectivity provided in Fig. 4, these nodes are:

$$\begin{aligned} r_k &= 1 + 2^p(k-1) \\ s_k &= 3 + 2^p(k-1) \end{aligned} \tag{10}$$

In the case of the double-expanded and the X-double-expanded octahedron ($p = 3$), Fig. 5, $r_1 = 1$, $s_1 = 3$, $r_2 = 9$, $s_2 = 11$, $r_3 = 17$, $s_3 = 19$. The length of this member, l_k, and its direction in space determine those of the rest of the struts in group k. The vector, $\mathbf{m}_k$, which characterize this director member is:

$$\mathbf{m}_k = \mathbf{X}_{s_k}^{\mathrm{T}} - \mathbf{X}_{r_k}^{\mathrm{T}} = \begin{pmatrix} x_{s_k} - x_{r_k} \\ y_{s_k} - y_{r_k} \\ z_{s_k} - z_{r_k} \end{pmatrix} \tag{11}$$

with $\mathbf{X}_r^{\mathrm{T}}$ as the vector of nodal coordinates of the r node. If e_r^i is the r-th component of the $\mathbf{e}^i$ vector ($i = \mathrm{I}, \cdots, \mathrm{VI}$) of the basis of ker$\mathbf{D}$, and the direction of $\mathbf{m}_k$ is given by the directional cosines, with θ_{j_k} ($j = x,y,z$, $k = 1, 2, 3$), angles, then, by considering the definition of nodal coordinates given in Eq. (5), Eq. (11) can be rewritten as:

$$\mathbf{m}_k = \begin{pmatrix} \sum_{i=1}^{\mathrm{Y}} \alpha_x^i \Delta e_{r_k s_k}^i \\ \sum_{i=1}^{\mathrm{Y}} \alpha_y^i \Delta e_{r_k s_k}^i \\ \sum_{i=1}^{\mathrm{Y}} \alpha_z^i \Delta e_{r_k s_k}^i \end{pmatrix} = l_k \begin{pmatrix} \cos\theta_{x_k} \\ \cos\theta_{y_k} \\ \cos\theta_{z_k} \end{pmatrix} \tag{12}$$

with $\Delta e_{r_k s_k}^i = e_{s_k}^i - e_{r_k}^i$.

Given that the self-weight of the members of tensegrity structures is not commonly considered when they are designed, the coordinates of the structure centroid $(\overline{x}\,\overline{y}\,\overline{z})^{\mathrm{T}}$ can be computed as the arithmetic mean of the structure nodal coordinates:

$$\overline{\mathbf{X}}^{\mathrm{T}} = \begin{pmatrix} \overline{x} \\ \overline{y} \\ \overline{z} \end{pmatrix} = \begin{pmatrix} \sum_{i=1}^{\mathrm{Y}} \alpha_x^i \overline{e}^i \\ \sum_{i=1}^{\mathrm{Y}} \alpha_y^i \overline{e}^i \\ \sum_{i=1}^{\mathrm{Y}} \alpha_z^i \overline{e}^i \end{pmatrix} \tag{13}$$

with $\overline{e}^i = \frac{1}{n}\sum_{r=1}^{n} e_r^i$ the average of coordinates of the $\mathbf{e}^i$ vector.

If the structural geometry is known a priori, i.e. $\overline{\mathbf{X}}$, l_k, and θ_{j_k} ($j = x,y,z, k = 1,2,3$) are known parameters, Eqs. (12) and (13) constitute a set of twelve equations where α_j^i ($j = x,y,z$, $i = \mathrm{I}, \cdots, \mathrm{IV}$) are the twelve unknown values to be solved. Furthermore, these twelve equations can be divided into three independent sets of four equations, each corresponding to each direction in space. Therefore, the three sets of four equations can be written in matrix form as:

$$\underbrace{\begin{pmatrix} \Delta e_{r_1 s_1}^{\mathrm{I}} & \Delta e_{r_1 s_1}^{\mathrm{II}} & \Delta e_{r_1 s_1}^{\mathrm{III}} & \Delta e_{r_1 s_1}^{\mathrm{IV}} \\ \Delta e_{r_2 s_2}^{\mathrm{I}} & \Delta e_{r_2 s_2}^{\mathrm{II}} & \Delta e_{r_2 s_2}^{\mathrm{III}} & \Delta e_{r_2 s_2}^{\mathrm{IV}} \\ \Delta e_{r_3 s_3}^{\mathrm{I}} & \Delta e_{r_3 s_3}^{\mathrm{II}} & \Delta e_{r_3 s_3}^{\mathrm{III}} & \Delta e_{r_3 s_3}^{\mathrm{IV}} \\ \overline{e}^{\mathrm{I}} & & \overline{e}^{\mathrm{II}} \overline{e}^{\mathrm{III}} \overline{e}^{\mathrm{IV}} & \end{pmatrix}}_{\mathbf{M}} \begin{pmatrix} \alpha_j^{\mathrm{I}} \\ \alpha_j^{\mathrm{II}} \\ \alpha_j^{\mathrm{III}} \\ \alpha_j^{\mathrm{VI}} \end{pmatrix} = \begin{pmatrix} l_1 \cos\theta_{j_1} \\ l_2 \cos\theta_{j_2} \\ l_3 \cos\theta_{j_3} \\ \bar{j} \end{pmatrix} \tag{14}$$

where $j = x,y,z$ and $\bar{j} = \overline{x}, \overline{y}, \overline{z}$. Matrix $\mathbf{M}$ in Eq. (14) is the matrix of coefficient of the three system of four linear equations (the same matrix for the three systems) and its construction depends on the vectors of the basis of ker$\mathbf{D}$, $\mathbf{e}^i$, with $i = \mathrm{I}, \cdots, \mathrm{IV}$. The resolution of the three systems of equations will be governed by the value of the determinant of the $\mathbf{M}$ matrix. Table 1 summarizes the values of the determinants of the $\mathbf{M}$ matrix in Eq. (14), for the full forms of both Octahedron and X-Octahedron families with $q_c = 1$ and $p \leq 12$. Values of $p > 12$ have not been evaluated due to computational limitations. As shown in Table 1, the determinant of $\mathbf{M}$ is non-zero in all studied cases.

Therefore, if Cramer's rule is applied, the twelve unknowns, α_j^i ($j = x, y, z$, $i = \mathrm{I}, \cdots, \mathrm{IV}$), can be obtained as:

$$\alpha_j^i = \frac{\det(\mathbf{M}_{ij})}{\det(\mathbf{M})} \tag{15}$$

where $\mathbf{M}_{ij}$ is the matrix formed by replacing the i-th column of $\mathbf{M}$ with the vector $\begin{pmatrix} l_1\cos\theta_{j_1} & l_2\cos\theta_{j_2} & l_3\cos\theta_{j_3} \end{pmatrix}^{\mathrm{T}}$. If $\det(\mathbf{M}_{ij})$ is computed by using Laplace's theorem from the i-th column, then α_j^i ($j = x,y,z, i = \mathrm{I}, \cdots,$ IV) is:

$$\alpha_j^i = \frac{(-1)^i}{\det(\mathbf{M})} \left(\sum_{k=1}^{3} [(-1)^k l_k \cos\theta_{j_k} \beta_{k,i}] + \bar{j}\beta_{4,i} \right) \tag{16}$$

where $\beta_{r,s}$ is the determinant of the matrix that results from removing row r and column s from the $\mathbf{M}$ matrix. In Eq. (16), the value of $i = \mathrm{I}, \cdots, \mathrm{IV}$ has been transformed to its Arabic counterpart in order to compute $(-1)^i$ or to select columns in the $\mathbf{M}$ matrix, and it is carried out in this way hereinafter.

According to the definition of α_j^i provided in Eq. (16), the α matrix can be written as:

$$\alpha = \alpha_c(\overline{x}, \overline{y}, \overline{z}) + \alpha_s(l_1, l_2, l_3, \theta_{x_1}, \theta_{y_1}, \theta_{z_1}, \theta_{x_2}, \theta_{y_2}, \theta_{z_2}, \theta_{x_3}, \theta_{y_3}, \theta_{z_3}) \tag{17}$$

where α_c is a matrix whose values only depend on the centroid coordinates, $(\overline{x}\,\overline{y}\,\overline{z})^{\mathrm{T}}$, and α_s is the tensegrity shape matrix whose elements are functions of the length and orientation of the struts in each group. Therefore, the definition of a tensegrity geometry needs the values of 12 parameters or 12 degrees of freedom (DOFs) to be set: $\overline{x}, \overline{y}, \overline{z}, l_1, l_2, l_3, \theta_{x_1}, \theta_{y_1}, \theta_{z_1}, \theta_{x_2}, \theta_{y_2}, \theta_{z_2}, \theta_{x_3}, \theta_{y_3}, \theta_{z_3}$. Given that neither the position of the tensegrity in space (determined by the coordinates of its centroid, $\overline{\mathbf{X}}$) nor its orientation as a rigid solid are significant when dealing with stability, the centroid of the structure is considered as the origin of the coordinates system, i.e. $\overline{\mathbf{X}} = (0 \quad 0 \quad 0)^{\mathrm{T}}$. From this point on, and without loss of generality, the struts of the $k = 1$ group are forced to be parallel to the x axis, members of the $k = 2$ group are placed on the $x-y$ plane, forming an angle of θ_{1-2} with members of the $k = 1$ group and, finally, members of the $k = 3$ group will be orientated in space so that they form angles of θ_{1-3} and θ_{2-3} with members of group (1) and (2), respectively. In doing so, $\mathbf{m}_k$ vectors, with $k = 1, 2, 3$ can be expressed as:

Table 1
Value of det($\mathbf{M}$) in terms of p for the full members of both the Octahedron and X-Octahedron families, with $q_c = 1$. Calculations have only been made up to $p = 12$ due to computational limitations.

p	det($\mathbf{M}$)	
	Oct	X-Oct
2	$6{,}30{\cdot}10^{6}$	$2{,}92{\cdot}10^{8}$
3	$1{,}09{\cdot}10^{7}$	$2{,}18{\cdot}10^{7}$
4	$-6{,}07{\cdot}10^{6}$	$-3{,}60{\cdot}10^{9}$
5	$1{,}21{\cdot}10^{9}$	$3{,}66{\cdot}10^{10}$
6	$-5{,}74{\cdot}10^{9}$	$-8{,}55{\cdot}10^{11}$
7	$5{,}55{\cdot}10^{10}$	$3{,}81{\cdot}10^{12}$
8	$-3{,}02{\cdot}10^{9}$	$-7{,}41{\cdot}10^{13}$
9	$2{,}05{\cdot}10^{12}$	$7{,}27{\cdot}10^{12}$
10	$-1{,}44{\cdot}10^{13}$	$-1{,}41{\cdot}10^{16}$
11	$1{,}81{\cdot}10^{12}$	$8{,}26{\cdot}10^{15}$
12	$-1{,}62{\cdot}10^{12}$	$-7{,}64{\cdot}10^{13}$

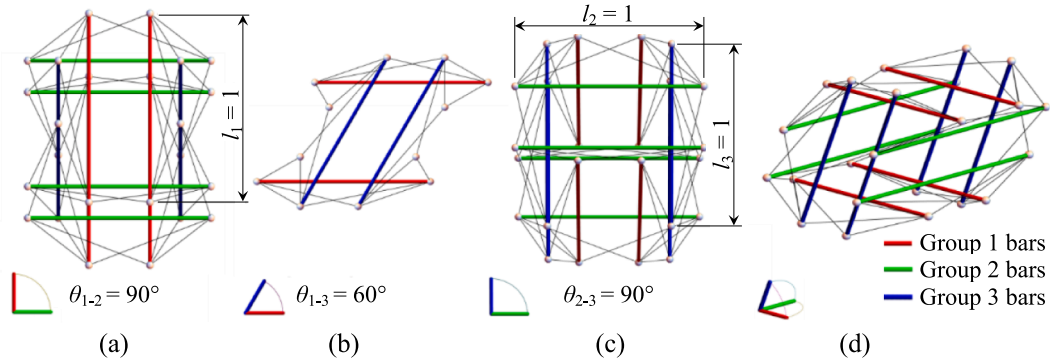

Fig. 7. Double-expanded octahedron ($p = 3$) with controlled geometry ($l_1 = l_2 = l_3 = 1$, $\theta_{1-2} = \theta_{2-3} = 90^{\circ}$, and $\theta_{1-3} = 60^{\circ}$): (a) normal view to plane 1–2, (b) normal view to plane 1–3, (c) normal view to plane 2–3, (d) 3D view.

$$\mathbf{m}_1 = l_1 \begin{pmatrix} 1 \\ 0 \\ 0 \end{pmatrix} \mathbf{m}_2 = l_2 \begin{pmatrix} \cos\theta_{1-2} \\ \sin\theta_{1-2} \\ 0 \end{pmatrix} \mathbf{m}_3 = l_3 \begin{pmatrix} \cos\theta_{1-3} \\ b \\ \sqrt{\sin^2\theta_{1-3} - b^2} \end{pmatrix} \tag{18}$$

with b as the factor obtained by establishing that the scalar product of the unit vectors that defines $\mathbf{m}_2$ and $\mathbf{m}_3$ equals $\cos\theta_{1-3}$, as indicated by Eq. (19):

$$\frac{\mathbf{m}_2}{l_2} \cdot \frac{\mathbf{m}_3}{l_2} = \cos\theta_{2-3} \rightarrow b = \frac{\cos\theta_{2-3} - \cos\theta_{1-2}\cos\theta_{1-3}}{\sin\theta_{1-2}} \in [-1, 1] \tag{19}$$

If all the above considerations are taken into account, only 6 DOFs need to be set for the definition of a tensegrity geometry: the length of each l_k ($k = 1, 2, 3$) group and the angles formed between each pair of groups: θ_{g-h} ($g = 1, 2$ and $h = 2, 3$ with $g \neq h$). Consequently, the α_c matrix is no longer needed and the terms of the α_s matrix can be computed by substituting the value of $\mathbf{m}_k$ vectors in Eqs. (14) and (16).

4.2. Examples of application

The cases of the double-expanded and the X-double-expanded octahedron ($p = 3$) are considered as examples of geometry control presented in this study. Their **C** connectivity matrices are obtained employing the plane connection graph presented in Fig. 5. A force:length ratio of $q_c = 1$ is assigned to cables, while $q_b = -4/3$ for the struts in the case of the double-expanded octahedron, Eq. (8), and $q_b = -7/5$ for the X-double-expanded octahedron, Eq. (9). The tensegrity cables and struts are numbered so that strut numbers are multiple of 5 in the Octahedron family and multiple of 6 in the X-Octahedron family. Therefore, the vector containing the force:length ratio of each member of the double expanded octahedron, $\mathbf{q}_{\text{Oct}} \in \mathbb{R}^{60}$, has the following structure:

$$\mathbf{q}_{\text{Oct}} = (1 \quad 1 \quad 1 \quad 1 \quad -4/3 \quad \cdots \quad 1 \quad 1 \quad 1 \quad 1 \quad -4/3)^T \tag{20}$$

and the vector of the X-double-expanded octahedron, $\mathbf{q}_{\text{X-Oct}} \in \mathbb{R}^{72}$, is:

$$\mathbf{q}_{\text{X-Oct}} = (1 \quad 1 \quad 1 \quad 1 \quad 1 \quad -7/5 \quad \cdots \quad 1 \quad 1 \quad 1 \quad 1 \quad 1 \quad -7/5)^T \tag{21}$$

After computing the $\mathbf{D} = \mathbf{C}^{\mathrm{T}} \cdot \mathbf{Q} \cdot \mathbf{C}$ force:length ratio matrix for both the double-expanded and the X-double expanded octahedron, the orthogonal basis of their null spaces is computed considering the eigenvectors that correspond to the 4 zero eigenvalues of the **D** matrix:

$$\begin{pmatrix} \mathbf{e}^{\mathrm{I}} & \mathbf{e}^{\mathrm{II}} & \mathbf{e}^{\mathrm{III}} & \mathbf{e}^{\mathrm{IV}} \end{pmatrix}_{\text{Oct}} = \begin{pmatrix} 1 & 155 & 45 & 17 \\ 5 & -127 & -17 & 11 \\ 1 & -91 & 63 & 35 \\ 5 & 119 & -35 & -7 \\ 5 & -127 & 27 & -1 \\ 1 & 155 & 1 & 29 \\ 5 & 119 & 9 & -19 \\ 1 & -91 & 19 & 47 \\ 2 & 105 & 83 & -1 \\ 4 & -77 & -55 & 29 \\ 2 & 105 & -49 & 35 \\ 4 & -77 & 77 & -7 \\ 2 & -59 & -37 & 47 \\ 4 & 87 & 65 & -19 \\ 2 & -59 & 95 & 11 \\ 4 & 87 & -67 & 17 \\ 0 & 82 & 82 & 29 \\ 6 & -54 & -54 & 1 \\ 6 & 28 & 28 & -28 \\ 0 & 0 & 0 & 56 \\ 6 & 28 & -60 & -4 \\ 0 & 0 & 88 & 32 \\ 0 & 82 & -6 & 50 \\ 6 & -54 & 34 & -22 \end{pmatrix} \begin{pmatrix} \mathbf{e}^{\mathrm{I}} & \mathbf{e}^{\mathrm{II}} & \mathbf{e}^{\mathrm{III}} & \mathbf{e}^{\mathrm{IV}} \end{pmatrix}_{\text{X-Oct}}$$

$$= \begin{pmatrix} 1 & 63 & 154 & 28 \\ 4 & -56 & -49 & 7 \\ 1 & -47 & 199 & 43 \\ 4 & 54 & -94 & -8 \\ 4 & -56 & 64 & -2 \\ 1 & 63 & 41 & 37 \\ 4 & 54 & 19 & -17 \\ 1 & -47 & 86 & 52 \\ 2 & 38 & 344 & -2 \\ 3 & -31 & -239 & 37 \\ 2 & 38 & -21 & 43 \\ 3 & -31 & 326 & -8 \\ 2 & -28 & -194 & 52 \\ 3 & 35 & 299 & -17 \\ 2 & -28 & 371 & 7 \\ 3 & 35 & -266 & 28 \\ 0 & 22 & 330 & 40 \\ 5 & -15 & -225 & -5 \\ 5 & 7 & 105 & -35 \\ 0 & 0 & 0 & 70 \\ 5 & 7 & -234 & -8 \\ 0 & 0 & 339 & 43 \\ 0 & 22 & -9 & 67 \\ 5 & -15 & 114 & -32 \end{pmatrix} \tag{22}$$

with these data, the $\alpha_{s_{\text{Oct}}}$ and $\alpha_{s_{\text{X-Oct}}}$ matrices can be built by using Eqs. (16), (18), and (19), remaining:

$$\alpha_{s_{\text{Oct}}} = \begin{pmatrix} \frac{7c_{x_3}l_3}{123} & \frac{7c_{y_3}l_3}{123} & \frac{7c_{z_3}l_3}{123} \\ -\frac{41c_{x_1}l_1+9c_{x_3}l_3}{10824} & -\frac{41c_{y_1}l_1+9c_{y_3}l_3}{10824} & -\frac{41c_{z_1}l_1+9c_{z_3}l_3}{10824} \\ \frac{3c_{x_1}l_1-22c_{x_2}l_2-9c_{x_3}l_3}{3696} & \frac{3c_{y_1}l_1-22c_{y_2}l_2-9c_{y_3}l_3}{3696} & \frac{3c_{z_1}l_1-22c_{z_2}l_2-9c_{z_3}l_3}{3696} \\ \frac{c_{x_1}l_1+2c_{x_2}l_2-3c_{x_3}l_3}{336} & \frac{c_{y_1}l_1+2c_{y_2}l_2-3c_{y_3}l_3}{336} & \frac{c_{z_1}l_1+2c_{z_2}l_2-3c_{z_3}l_3}{336} \end{pmatrix} \quad (23)$$

$$\alpha_{s_{\text{X-Oct}}} = \begin{pmatrix} \frac{7c_{x_3}l_3}{110} & \frac{7c_{y_3}l_3}{110} & \frac{7c_{z_3}l_3}{110} \\ -\frac{22c_{x_1}l_1+3c_{x_3}l_3}{2486} & -\frac{22c_{y_1}l_1+3c_{y_3}l_3}{2486} & -\frac{22c_{z_1}l_1+3c_{z_3}l_3}{2486} \\ \frac{9c_{x_1}l_1-113c_{x_2}l_2-45c_{x_3}l_3}{79100} & \frac{9c_{y_1}l_1-113c_{y_2}l_2-45c_{y\_3}l_3}{79100} & \frac{9c_{z_1}l_1-113c_{z_2}l_2-45c_{z_3}l_3}{79100} \\ \frac{c_{x_1}l_1+3c_{x_2}l_2-5c_{x_3}l_3}{700} & \frac{c_{y_1}l_1+3c_{y_2}l_2-5c_{y_3}l_3}{700} & \frac{c_{z_1}l_1+3c_{z_2}l_2-5c_{z_3}l_3}{700} \end{pmatrix}$$

with $c_{x_1}=1$, $c_{y_1}=c_{z_1}=0$, $c_{x_2}=\cos\theta_{1-2}$, $c_{y_2}=\sin\theta_{1-2}$, $c_{z_2}=0$, $c_{x_3}=\cos\theta_{1-3}$, $c_{y_3}=\frac{\cos\theta_{2-3}-\cos\theta_{1-2}\cos\theta_{1-3}}{\sin\theta_{1-2}}\in[-1,1]$, and $c_{z_3}=\sqrt{\sin^2\theta_{1-3}-{c_{y_3}}^2}$, according to Eqs. (18) and (19). The expression of the $\alpha_{s_{\text{Oct}}}$ and $\alpha_{s_{\text{X-Oct}}}$ matrices for other members of the Octahedron and X-Octahedron families are given in Appendix 1, together with the $\mathbf{e}^i$ vectors employed to get them. Fig. 7 shows a realization of the double-expanded octahedron in which all the struts have the same length, ($l_k=1$), groups 1 and 2, and groups 2 and 3 are perpendicular to each other, and groups 1 and 3 form an angle of 60° (i.e. $\theta_{1-3}=60^\circ$). However, Fig. 8 shows a realization of the X-double-expanded octahedron in which the struts in groups 1 and 3 have unit length, while those in group (2) have half the length (i.e., $l_2=1/2$). In the structure represented in Fig. 8, $\theta_{1-2}=90^\circ$, $\theta_{1-3}=80^\circ$, and $\theta_{2-3}=45^\circ$.

5. Stability of folded forms

Eqs. (8) and (9) establish the relationship between the force:length ratios of the struts (q_b) and the cables (q_c) corresponding to the p-th member full form equilibrium configuration in the Octahedron and the X-Octahedron families, respectively. Hereinafter, the value of p that leads to the full form of the p −th member will be referred to as p_{full}. It has been also stated that all the previous members are obtained in their folded form from the connectivity patter of the p_{full}-th member of the tensegrity family. The q_b/q_c ratios corresponding to these folded forms are obtained by introducing $p_{\text{folded}}=p_{\text{full}}-\psi$, $\psi\in\Psi=\left\{\psi\in\mathbb{Z}:1\le\psi<p_{\text{full}}\right\}$, in Eqs. (8) or (9) [40].

5.1. Super-stability

The main advantage of obtaining a super-stable tensegrity structure is that it remains stable regardless the material used its members (cables and struts). Additionally, if the structure is super-stable for a particular force:length ratios assignment, it is always stable regardless the applied level of pre-stress [39].

As observed in the previous works dealing with the Octahedron and the X-Octahedron families, all the folded forms represented always resulted as non-super-stable examples [34,36,37,40]. Therefore, the options for creating a super-stable folded form are analyzed for both the Octahedron and X-Octahedron families.

Let the connectivity pattern of the p_{full} member of either Octahedron or X-Octahedron families be considered. Let $\mathbf{C}_{p_{\text{full}}}\in\mathbb{R}^{m_{p_{\text{full}}}\times n_{p_{\text{full}}}}$ be the connectivity matrix and $\mathbf{Q}_{(p_{\text{folded}},p_{\text{full}})}\in\mathbb{R}^{m_{p_{\text{full}}}\times m_{p_{\text{full}}}}$ be the diagonal matrix with the force:length ratio assignment that corresponds to $q_c=1$ and

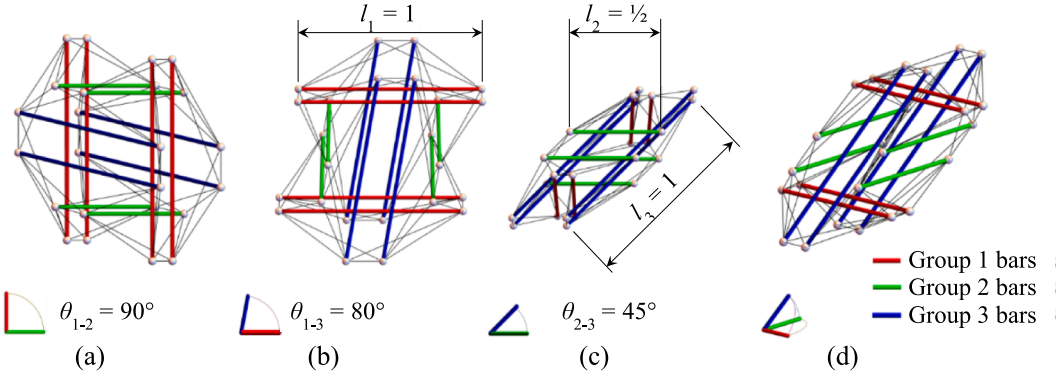

Fig. 8. X-double-expanded octahedron ($p=3$) with controlled geometry ($l_1=l_3=1$, $l_2=1/2$, $\theta_{1-2}=90^\circ$, $\theta_{1-3}=80^\circ$, and $\theta_{2-3}=45^\circ$): (a) normal view to plane 1–2, (b) normal view to plane 1–3, (c) normal view to plane 2–3, (d) 3D view.

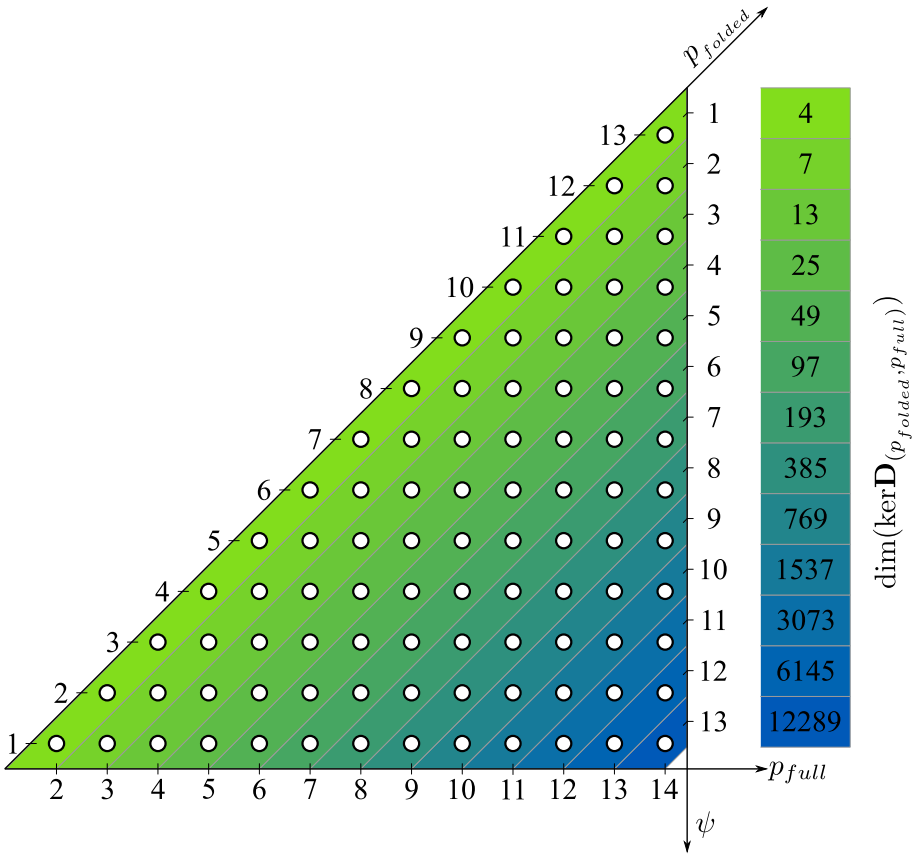

Fig. 9. Dimension of null space of $\mathbf{D}_{(p_{\text{folded}},p_{\text{full}})}$ matrix corresponding to the p_{folded}-th member as a folded form of p_{full}-th member, for both Octahedron and X-Octahedron families. Calculations are shown up to $p_{\text{full}} = 14$ due to computational limitations.

the q_b/q_c ratio obtained by introducing $p_{\text{folded}} = p_{\text{full}} - \psi$, $\psi \in \Psi = \left\{\psi \in \mathbb{Z} : 1 \leq \psi < p_{\text{full}}\right\}$ in Eq. (8) for the Octahedron family and Eq. (9) for the X-Octahedron family. Let the $\mathbf{D}_{(p_{\text{folded}},p_{\text{full}})} \in \mathbb{R}^{n_{p_{\text{full}}} \times n_{p_{\text{full}}}}$ matrix be considered as the force density matrix of the p_{folded}-th member as a folded form of the p_{full}-th member, calculated as:

$$\mathbf{D}_{(p_{\text{folded}},p_{\text{full}})} = \mathbf{C}_{p_{\text{full}}}^{\text{T}} \cdot \mathbf{Q}_{(p_{\text{folded}},p_{\text{full}})} \cdot \mathbf{C}_{p_{\text{full}}} \tag{24}$$

The condition according to which the rank deficiency of the $\mathbf{D}_{(p_{\text{folded}},p_{\text{full}})}$ matrix must be 4 is studied in Fig. 9, with calculations made up to $p_{\text{full}} = 14$ because of computational limitations. The rank deficiency of the matrix $\mathbf{D}_{(p_{\text{folded}},p_{\text{full}})}$ that corresponds to p_{folded}-th member as a folded form of the p_{full}-th member, or the dimension of $\ker\mathbf{D}_{(p_{\text{folded}},p_{\text{full}})}$, is:

$$\dim\left(\ker\mathbf{D}_{(p_{\text{folded}},p_{\text{full}})}\right) = 3{\cdot}2^{\psi-1} + 1 \tag{25}$$

with $\psi \in \Psi = \left\{\psi \in \mathbb{Z} : 1 \leq \psi < p_{\text{full}}\right\}$. When considering a pair of p_{full} and p_{folded} values there is no difference between the rank deficiency of the $\mathbf{D}_{(p_{\text{folded}},p_{\text{full}})}$ matrix for both the Octahedron and X-Octahedron families. Fig. 9 also shows that when $\psi > 1$, i.e. folded forms beyond the previous one to the p_{full}-th member, the super-stability condition to the rank deficiency of the $\mathbf{D}$ matrix is not fulfilled.

The condition which the $\mathbf{D}$ matrix needs to be positive semi-definite is considered here. Fig. 10 shows the minimum eigenvalue of the $\mathbf{D}_{(p_{\text{folded}},p_{\text{full}})}$ matrix for the Octahedron family (with q_b/q_c given by Eq. (8), Fig. 10(a) and (c)) and for the X-Octahedron family (with q_b/q_c given by Eq. (9), Fig. 10(b) and (d)). Calculations are again made up to $p_{\text{full}} = 14$ because of computational limitations. Each curve in Fig. 10(a) and (b) represents the minimum eigenvalue of $\mathbf{D}_{(p_{\text{folded}},p_{\text{full}})}$ as a function of p_{full} for a fixed value of p_{folded}. All the curves have a negative horizontal asymptote as p_{full} increases. However, the curves in Fig. 10(c) and (d) represent the minimum eigenvalue of $\mathbf{D}_{(p_{\text{folded}},p_{\text{full}})}$ as a function of p_{full} for fixed values of $\psi = p_{\text{full}} - p_{\text{folded}}$. These curves indicate that, for a particular value of ψ, the minimum eigenvalue of $\mathbf{D}_{(p_{\text{folded}},p_{\text{full}})}$ increases as p_{full} increases, but it is always negative, with an asymptote in 0. Particularly interesting is the curve that corresponds to $\psi = 1$, for which the $\boldsymbol{D}_{(p_{\text{folded}},p_{\text{full}})}$ force density matrix always has a rank deficiency of 4, Fig. 9 (Eq. (25)). For this case, the minimum eigenvalue of $\mathbf{D}_{(p_{\text{folded}},p_{\text{full}})}$ is the closest to 0, but it is negative, so $\mathbf{D}_{(p_{\text{folded}},p_{\text{full}})}$ is never positive semi-definite.

Therefore, it can be concluded that folded forms of the Octahedron and X-Octahedron families can never be super-stable as the corresponding $\mathbf{D}_{(p_{\text{folded}},p_{\text{full}})}$ matrix does not have a rank deficiency equal to 4, and/or it is not positive semi-definite.

5.2. Stability by geometry control

The linear combination of vectors of the basis of $\ker\mathbf{D}$, $\mathbf{e}^i$, $(i = \text{I}, \cdots, \text{IV})$, adopted to obtain the geometry of the structure, has a significant influence when dealing with the stability of the folded forms of both Octahedron and X-Octahedron families [40]. In fact, this linear combination could lead to either a stable or an unstable tensegrity structure. Therefore, a study of this influence is worth performing.

A tensegrity structure is stable if its $\mathbf{K} \in \mathbb{R}^{3n}$ tangent stiffness matrix is positive definite, and if the 6 null eigenvalues that corresponds to its rigid solid motions in space [1] are not considered. As explained in [1,37], the tangent stiffness matrix is computed as the sum of the $\mathbf{K}_{\text{E}}$

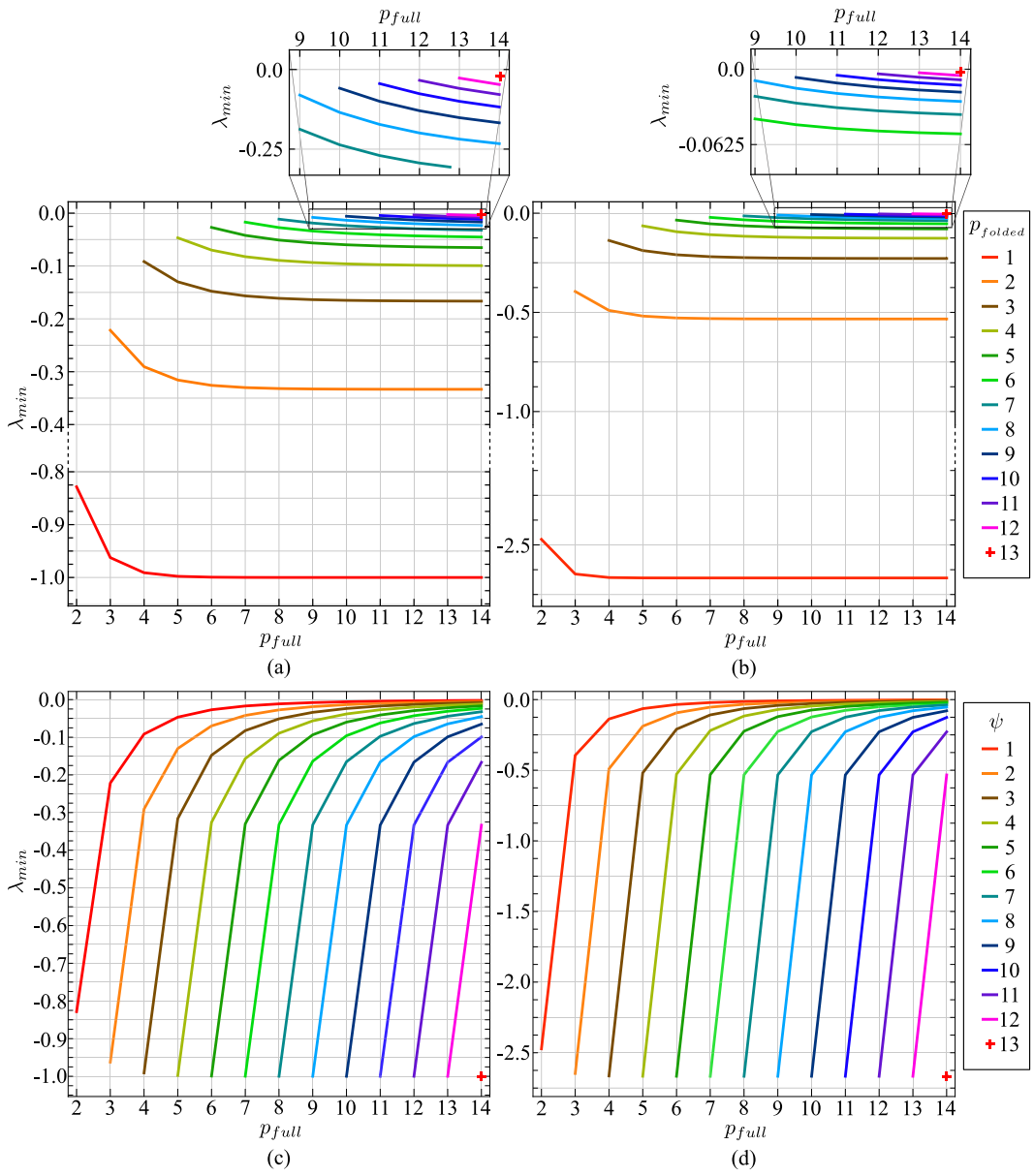

Fig. 10. Minimum eigenvalue λ_{min} of matrix $\mathbf{D}_{(p_{\text{folded}}, p_{\text{full}})}$ as a function of p_{full}: for fixed values of p_{folded} ((a) for Octahedron and (b) for the X-Octahedron families), and for fixed values of $\psi = p_{\text{full}} - p_{\text{folded}}$ (c) for Octahedron and (d) for the X-Octahedron families). Calculations are shown up to $p_{\text{full}} = 14$ due to computational limitations.

elastic stiffness matrix and the $\mathbf{K}_{\text{G}}$ geometric stiffness matrix, meaning that $\mathbf{K} = \mathbf{K}_{\text{E}} + \mathbf{K}_{\text{G}}$. If $\mathbf{A} \in \mathbb{R}^{3n \times m}$ is the equilibrium matrix of the tensegrity [37], $\mathbf{A}$ could be defined as:

$$\mathbf{A} = \begin{pmatrix} \mathbf{C}^{\text{T}}\text{diag}(\mathbf{C}\cdot\mathbf{x}) \\ \mathbf{C}^{\text{T}}\text{diag}(\mathbf{C}\cdot\mathbf{y}) \\ \mathbf{C}^{\text{T}}\text{diag}(\mathbf{C}\cdot\mathbf{z}) \end{pmatrix} \tag{26}$$

Then, the elastic stiffness matrix, $\mathbf{K}_{\text{E}}$, in the global coordinate system can be written as:

$$\mathbf{K}_{\text{E}} = \mathbf{A}\cdot\boldsymbol{diag}\left(\frac{E_k \Omega_k}{\left(L_k^0\right)^3}\right)\cdot\mathbf{A}^T \tag{27}$$

where E_k, Ω_k, and L_k^0 are the Young modulus, the cross-sectional area and the initial length of the $k = 1, \cdots, m$ member, respectively. The $\mathbf{K}_{\text{G}}$ geometric stiffness matrix is written employing the tensor product (Kronecker product), $\otimes$, as:

$$\mathbf{K}_{\text{G}} = \mathbf{I}_3 \otimes \mathbf{D} \tag{28}$$

The folded forms of the Octahedron and X-Octahedron families can be stable or unstable depending on the linear combinations of vectors of the basis of ker$\mathbf{D}$ considered ($\mathbf{e}^i$, with $i = \text{I}, \cdots, \text{IV}$) [40]. Section 4 shows that this linear combination is explicitly related to the position of the structure in space and to its shape, which is the key aspect of structural stability. Once the force:length ratio of each member of the tensegrity is known (Eqs. (8) or (9)) and the shape of the structure is assigned (Eqs. (16), (18), and (19)), the $\mathbf{K}_{\text{E}}$ and $\mathbf{K}_{\text{G}}$ matrices can be computed and the stability analysis performed. This analysis enables the designer to discover the range of values of the 6 variables controlling the geometry of the structure (the length of each group l_k ($k = 1, 2, 3$) and the angles formed between each pair of groups: θ_{g-h} ($g = 1, 2$ and $h = 2, 3$ with $g \neq h$), which lead to a stable tensegrity.

As an example of application, the stability analysis of the expanded octahedron and the X-expanded octahedron ($p_{\text{folded}} = 2$) as folded forms

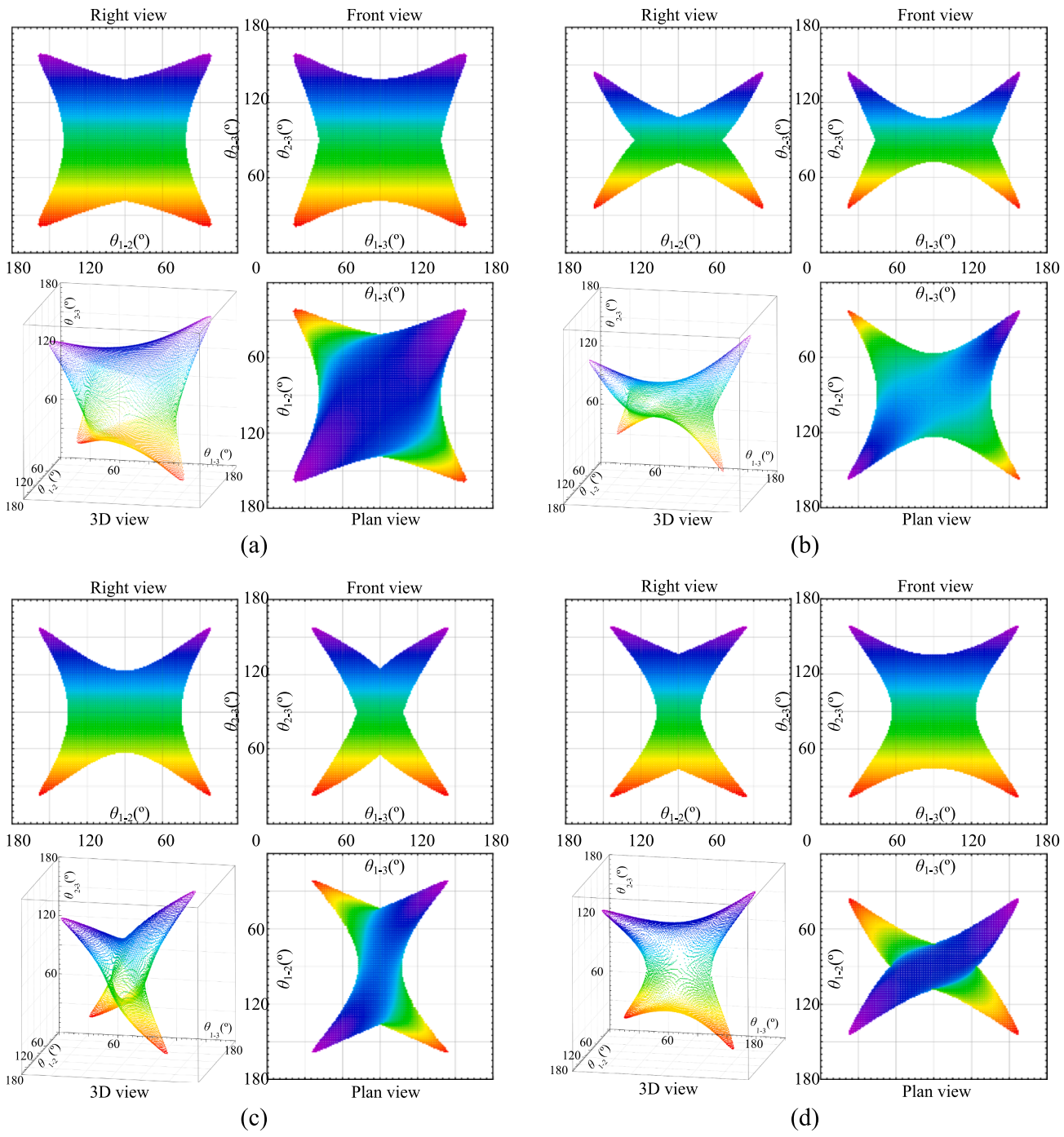

Fig. 11. 3D, right, front, and plan views of the region of values (θ_{1-2}, θ_{1-3}, θ_{2-3}) that provide a stable expanded octahedron ($p_{\text{folded}} = 2$) as a folded form of the double-expanded octahedron ($p_{\text{full}} = 3$) in the Octahedron family with different lengths of groups of struts: (a) $l_1 = l_2 = l_3 = 1$, (b) $l_1 = 2$, $l_2 = l_3 = 1$, (c) $l_1 = l_3 = 1$, $l_2 = 2$, and (d) $l_1 = l_2 = 1$, $l_3 = 2$. Colors are added to the represented solutions to better identify them in the different presented views of the regions.

of the double expanded octahedron and the X-double-expanded octahedron ($p_{\text{full}} = 3$), respectively, are presented. All the cables have a force:length ratio of $q_c = 1$ and the struts are assigned a force:length ratio obtained from Eq. (8) ($q_b = -\frac{(3-1)+1}{(3-1)} = -\frac{3}{2}$, for the expanded octahedron) and Eq. (9) ($q_b = -\frac{2(3-1)+1}{2(3-1)-1} = -\frac{5}{3}$, for the X-expanded octahedron). The vectors of the basis of ker$\mathbf{D}$ and the α_s matrices required to obtain the geometries of the structures are given in Appendix 1. Four different studies are performed for each structure, and the lengths of the l_k ($k = 1, 2, 3$) groups are always fixed, and the θ_{1-2}, θ_{1-3}, and θ_{2-3} angles are modified. In the first study, all the lengths are equal to one, $l_k = 1$ ($k = 1, 2, 3$), while in the other cases, one of the groups has a length of 2, and the others have a length of 1. The computations are made by assuming the structures are built in steel, i.e., $E_k = 200$, GPa, and the Ω_k cross sectional areas of both cables and struts are such that the maximum prestress in both types of elements equals 1 % of the $E_k\Omega_k$ product, as suggested by [1] for conventional tensegrity structures. Fig. 11 and Fig. 12 show the θ_{1-2}, θ_{1-3}, and θ_{2-3} ranges of values for which the folded forms of the Octahedron and the X-Octahedron families, respectively, are stable for the lengths of the groups of struts considered.

The first aspect that stands out when comparing Fig. 11 and Fig. 12 is that regions of stable structures are similar but more voluminous in the

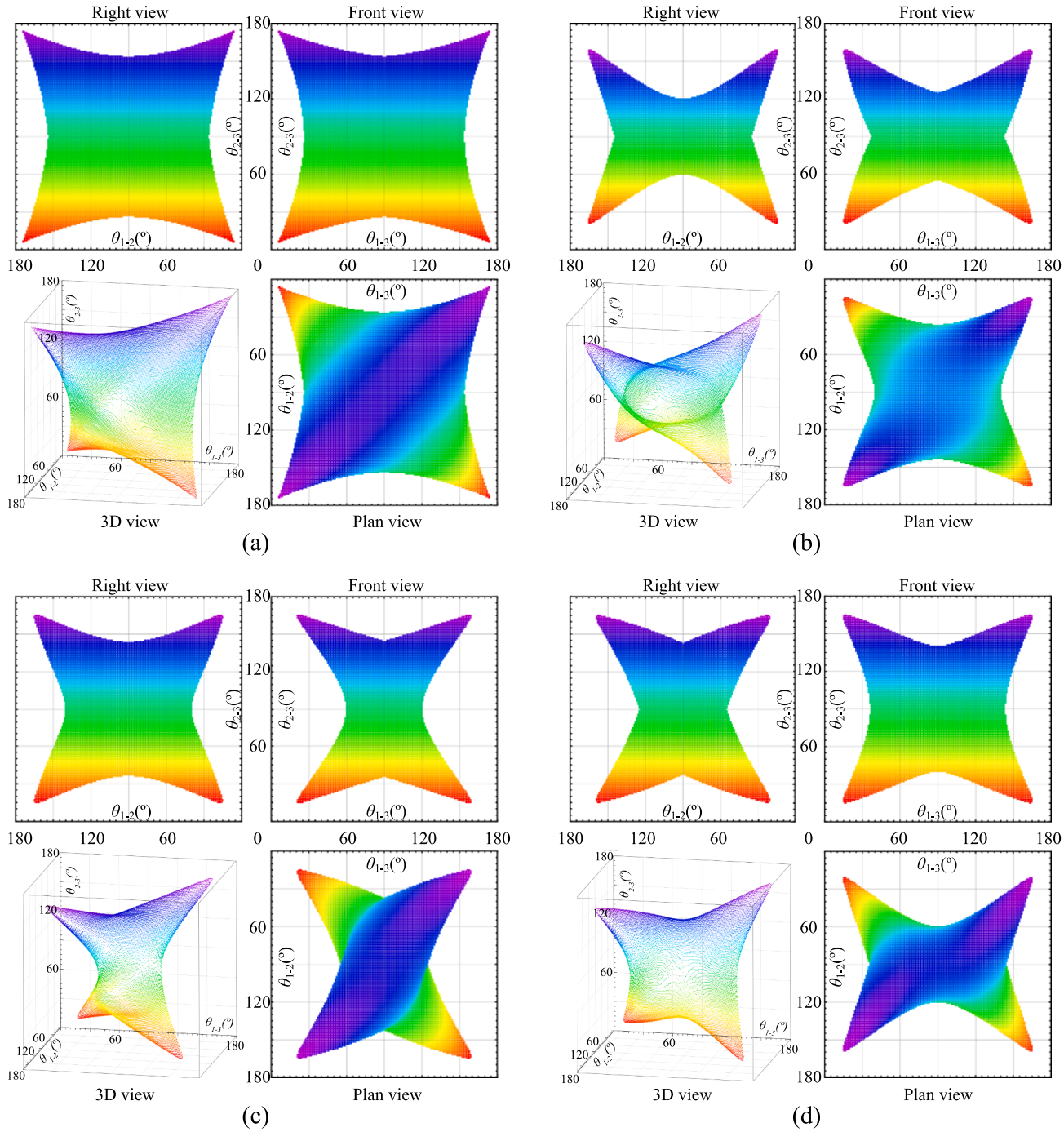

Fig. 12. 3D, right, front, and plan views of the region of values (θ_{1-2}, θ_{1-3}, θ_{2-3}) that provide a stable X-expanded octahedron ($p_{\text{folded}} = 2$) as a folded form of the X-double-expanded octahedron ($p_{\text{full}} = 3$) in the Octahedron family with different lengths of groups of struts: (a) $l_1 = l_2 = l_3 = 1$, (b) $l_1 = 2$, $l_2 = l_3 = 1$, (c) $l_1 = l_3 = 1$, $l_2 = 2$, and (d) $l_1 = l_2 = 1$, $l_3 = 2$.

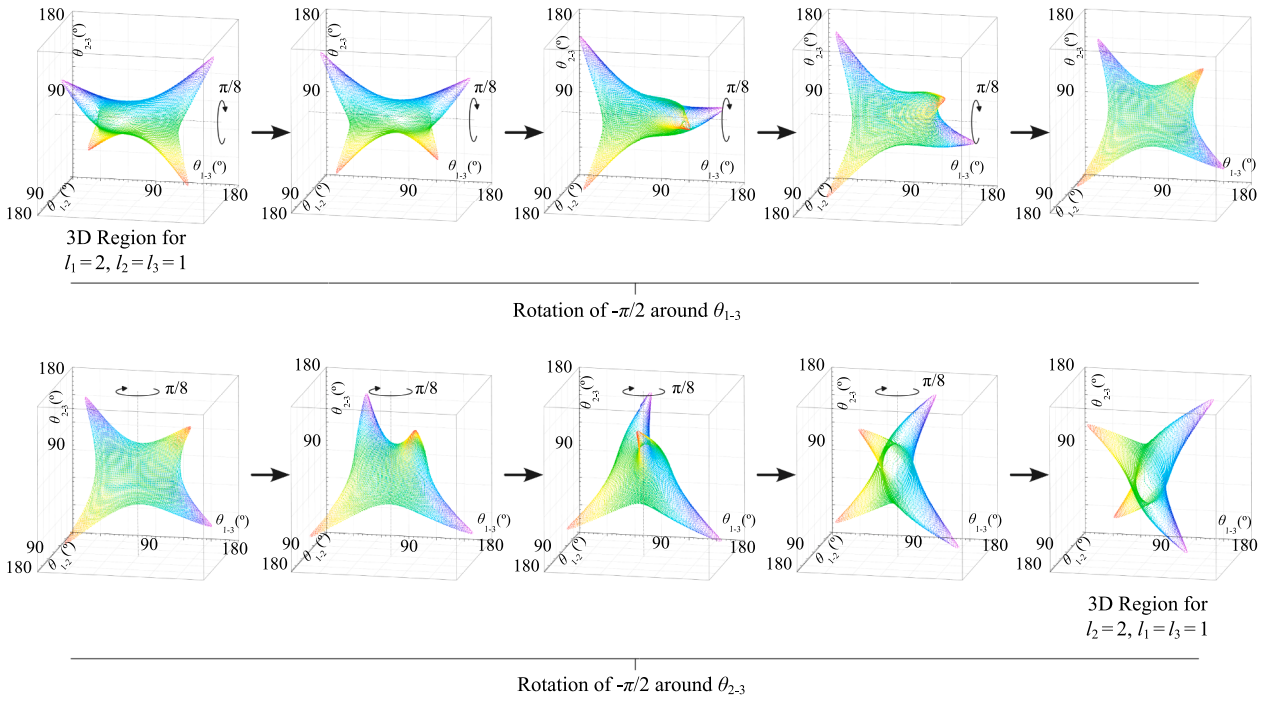

Fig. 13. Rotations of region of stable solutions for the expanded octahedron as a folded form of the double-expanded octahedron when $l_1 = 2, l_2 = l_3 = 1$ (Fig. 11 (b)), to get the region of stable solutions corresponding to $l_1 = l_3 = 1, l_2 = 2$ (Fig. 11(c)).

Table 2
Correspondence between the axes of the different 3D regions of stable solutions when one of the groups has twice the length of the others, Fig. 11 and Fig. 12(b), (c), and (d).

$l_1 - l_2 - l_3$		
2-1-1	1-2-1	1-1-2
θ_{1-2}	θ_{2-3}	θ_{1-3}
θ_{1-3}	θ_{1-2}	θ_{2-3}
θ_{2-3}	θ_{1-3}	θ_{1-2}

X-Octahedron family. In other words, there are more combinations of the θ_{1-2}, θ_{1-3}, and θ_{2-3} angles that lead to stable tensegrities, indicating that the additional cable in the basic rhombic cell, Fig. 1(b), provides stability to the structure. Another important aspect for both families is that there are more stable solutions when the same length is employed for all the groups of struts in the structure, suggesting that shorter struts lead to more stable structures.

Finally, an important finding for both families is that, when comparing the cases where the length of one of the groups if twice as long as the lengths of the others (Fig. 11 and Fig. 12(b), (c) and (d)), it becomes evident that the region of stable solutions is the same in all three cases, but in a rotated form. That is why the four different views of the regions in Fig. 11 and Fig. 12(b), (c) and (d) have been included. If the region that corresponds to $l_1 = 2, l_2 = l_3 = 1$ in Fig. 11(b) is first rotated by $-\pi/2$ around the θ_{1-3} axis and the region around the θ_{1-2} axis is rotated by $-\pi/2$, the region of stable solutions that corresponds to $l_1 = l_3 = 1, l_2 = 2$ presented in Fig. 11(c) is obtained, as shown in Fig. 13. The correspondence between angles θ_{1-2}, θ_{1-3}, and θ_{2-3} for the cases $l_1 = 2, l_2 = l_3 = 1$, $l_1 = l_3 = 1, l_2 = 2$, and $l_1 = l_2 = 1, l_3 = 2$ is summarized in Table 2. This table presents an important result, as it indicates that having the 3D region corresponding to one of cases (e.g., $l_1 = 2, l_2 = l_3 = 1$), the 3D region corresponding the other two cases can be obtained by only changing the axis indicated in Table 2, with major computations savings.

6. Conclusions

The FDM has been employed to get the equilibrium configuration of tensegrity structures from the Octahedron and X-Octahedron families. The final spatial realization of such structures depends on the linear combination of vectors that constitute a basis of the null space of the **D** tensegrity force density matrix. However, it is difficult to control the final geometry of the structure by directly changing the parameters involved in the linear combination of these vectors.

A new analytical formulation that enables the designer to control the shape of the tensegrity has been provided for the Octahedron and the X-Octahedron families. The formulation is based on the fact that all the struts in the structures of these families are grouped into three distinct sets, with the struts in each set having the same lengths and spatial orientations. Depending on the specific member of the Octahedron or X-Octahedron families to be obtained, this formulation defines the parameters to be used in the linear combination of the vectors. These parameters are defined in terms of both the lengths of each group of struts and the angles between these groups, allowing for complete control over the structure's geometry. Controlling the geometry of these types of tensegrities is essential for their use in the construction industry, such as in the form of simple modules that can be connected to build larger structures. In addition to the new formulation for geometry control, it has been proven that the folded forms of tensegrities in the Octahedron and X-Octahedron families can never be super-stable, which is a novel finding in the literature.

Tensegrity geometry is not relevant when considering the super-stability of the structure. However, this work has shown that geometry becomes important when evaluating whether a structure is stable or unstable, which is a key factor in construction of a tensegrity structure. As demonstrated, folded forms in the Octahedron and X-Octahedron families can be considered stable if certain geometric conditions are met. For fixed lengths of the groups of struts, there are closed regions of stable solutions defined by the angles formed between each group of struts ($\theta_{1-2}, \theta_{1-3}$, and θ_{2-3}). Examples of these regions have been presented for both the expanded octahedron as a folded form of the double-expanded octahedron and for the X-expanded octahedron as a folded form of the X-double expanded octahedron. The examples indicate that the longer struts groups, the fewer stable solutions exist. Furthermore, when comparing the regions of stable solutions for the Octahedron and the X-Octahedron families, the additional cable in the X-Octahedron's rhombic cell enhances stability for given strut lengths. Finally, it has been shown that the 3D regions obtained in the θ_{1-2}, θ_{1-3}, and θ_{2-3} space are the same in all three cases, but they are rotated around specific axes. Therefore, once one of the 3D regions has been computed, the other two can be obtained by simply applying the corresponding rotations, leading to significant computational savings.

CRediT authorship contribution statement

J.F. Carbonell-Márquez: Writing – original draft, Visualization, Methodology, Investigation, Formal analysis, Conceptualization. **M.A. Fernández-Ruiz:** Writing – review & editing, Investigation, Formal analysis, Conceptualization. **E. Hernández-Montes:** Writing – review & editing, Validation, Supervision. **L.M. Gil-Martín:** Writing – review & editing, Validation, Supervision.

Declaration of competing interest

The authors declare that they have no known competing financial interests or personal relationships that could have appeared to influence the work reported in this paper.

Data availability

Data will be made available on request.

Acknowledgments

The present paper was financed by the Ministry of Science, Innovation and Universities of Spain under the research projects with references PID2023-150724OB-C21 and PID2023-150724OA-C22. The publication charges for this work as open access have been covered by Universidad de Málaga /CBUA. Their support is gratefully acknowledged.

Appendix 1

Some possible bases of ker**D** and the corresponding α_s matrices to control the shape of 2 first member of both Octahedron and X-Octahedron families are indicated below. For the double-expanded octahedron and X-double-expanded octahedron are given in Eqs. (22) and (23). Connectivity between nodes can be calculated from Fig. 2 and Fig. 4:

- Octahedron and X-octahedron ($p = 1$)

$$\begin{pmatrix} \mathbf{e}^{\mathrm{I}} & \mathbf{e}^{\mathrm{II}} & \mathbf{e}^{\mathrm{III}} & \mathbf{e}^{\mathrm{IV}} \end{pmatrix} = \begin{pmatrix} 1 & 1 & 2 & -2 \\ 0 & 0 & 0 & 4 \\ 1 & 1 & -3 & 1 \\ 0 & 0 & 5 & 1 \\ 0 & 3 & 1 & 1 \\ 1 & -2 & 1 & 1 \end{pmatrix}$$

$$\alpha_s = \begin{pmatrix} -\frac{c_{x_1} l_1 + c_{x_2} l_2 - c_{x_3} l_3}{6} & -\frac{c_{y_1} l_1 + c_{y_2} l_2 - c_{y_3} l_3}{6} & -\frac{c_{z_1} l_1 + c_{z_2} l_2 - c_{z_3} l_3}{6} \\ -\frac{c_{x_1} l_1 + c_{x_2} l_2 + 5c_{x_3} l_3}{30} & -\frac{c_{y_1} l_1 + c_{y_2} l_2 + 5c_{y_3} l_3}{30} & -\frac{c_{z_1} l_1 + c_{z_2} l_2 + 5c_{z_3} l_3}{30} \\ \frac{-c_{x_1} l_1 + 4c_{x_2} l_2}{40} & \frac{-c_{y_1} l_1 + 4c_{y_2} l_2}{40} & \frac{-c_{z_1} l_1 + 4c_{z_2} l_2}{40} \\ \frac{c_{x_1} l_1}{8} & \frac{c_{y_1} l_1}{8} & \frac{c_{z_1} l_1}{8} \end{pmatrix} \tag{29}$$

- Expanded octahedron ($p = 2$)

$$\left(\mathbf{e}^{\mathrm{I}} \quad \mathbf{e}^{\mathrm{II}} \quad \mathbf{e}^{\mathrm{III}} \quad \mathbf{e}^{\mathrm{IV}}\right) = \begin{pmatrix} 7 & 7 & -7 & -1 \\ -3 & -77 & 77 & 11 \\ -1 & -149 & -3 & 11 \\ 5 & 79 & 73 & -1 \\ 4 & 78 & -2 & 14 \\ 0 & -148 & 72 & -4 \\ 4 & -70 & 70 & -10 \\ 0 & 0 & 0 & 20 \\ 4 & -70 & -63 & 11 \\ 0 & 0 & 133 & -1 \\ 0 & 74 & 97 & 11 \\ 4 & -144 & -27 & -1 \end{pmatrix} \tag{30}$$

$$\alpha_s = \begin{pmatrix} -\dfrac{10c_{x_1}l_1 + 5c_{x_2}l_2}{148} & -\dfrac{10c_{y_1}l_1 + 5c_{y_2}l_2}{148} & -\dfrac{10c_{z_1}l_1 + 5c_{z_2}l_2}{148} \\ -\dfrac{39c_{x_1}l_1 + 37c_{x_2}l_2 - 36c_{x_3}l_3}{19648} & -\dfrac{39c_{y_1}l_1 + 37c_{y_2}l_2 - 36c_{y_3}l_3}{19648} & -\dfrac{39c_{z_1}l_1 + 37c_{z_2}l_2 - 36c_{z_3}l_3}{19648} \\ \dfrac{c_{x_1}l_1 + 18c_{x_2}l_2 + 40c_{x_3}l_3}{10640} & \dfrac{c_{y_1}l_1 + 18c_{y_2}l_2 + 40c_{y_3}l_3}{10640} & \dfrac{c_{z_1}l_1 + 18c_{z_2}l_2 + 40c_{z_3}l_3}{10640} \\ \dfrac{c_{x_1}l_1 - 2c_{x_2}l_2}{80} & \dfrac{c_{y_1}l_1 - 2c_{y_2}l_2}{80} & \dfrac{c_{z_1}l_1 - 2c_{z_2}l_2}{80} \end{pmatrix}$$

- X-expanded octahedron ($p = 2$)

$$\left(\mathbf{e}^{\mathrm{I}} \quad \mathbf{e}^{\mathrm{II}} \quad \mathbf{e}^{\mathrm{III}} \quad \mathbf{e}^{\mathrm{IV}}\right) = \begin{pmatrix} 13 & -13 & 13 & 1 \\ -7 & -247 & 247 & 19 \\ -5 & -376 & 7 & 19 \\ 11 & 116 & 253 & 1 \\ 6 & 121 & 2 & 34 \\ 0 & -381 & 258 & -14 \\ 6 & -260 & 260 & -20 \\ 0 & 0 & 0 & 40 \\ 6 & -260 & -273 & 19 \\ 0 & 0 & 533 & 1 \\ 0 & 127 & 447 & 19 \\ 6 & -387 & -187 & 1 \end{pmatrix} \tag{31}$$

$$\alpha_s = \begin{pmatrix} -\dfrac{15c_{x_1}l_1 + 5c_{x_3}l_3}{381} & -\dfrac{15c_{y_1}l_1 + 5c_{y_3}l_3}{381} & -\dfrac{15c_{z_1}l_1 + 5c_{z_3}l_3}{381} \\ -\dfrac{121c_{x_1}l_1 + 127c_{x_2}l_2 - 129c_{x_3}l_3}{203073} & -\dfrac{121c_{y_1}l_1 + 127c_{y_2}l_2 - 129c_{y_3}l_3}{203073} & -\dfrac{121c_{z_1}l_1 + 127c_{z_2}l_2 - 129c_{z_3}l_3}{203073} \\ \dfrac{-c_{x_1}l_1 + 43c_{x_2}l_2 + 120c_{x_3}l_3}{127920} & \dfrac{-c_{y_1}l_1 + 43c_{y_2}l_2 + 120c_{y_3}l_3}{127920} & \dfrac{-c_{z_1}l_1 + 43c_{z_2}l_2 + 120c_{z_3}l_3}{127920} \\ \dfrac{c_{x_1}l_1 - 3c_{x_2}l_2}{240} & \dfrac{c_{y_1}l_1 - 3c_{y_2}l_2}{240} & \dfrac{c_{z_1}l_1 - 3c_{z_2}l_2}{240} \end{pmatrix}$$

The vectors of the basis of ker$\mathbf{D}$ and the corresponding α_s matrices employed to obtain the geometries of the expanded octahedron as a folded form of the double-expanded octahedron and the X-expanded-octahedron as a folded form of the X-double-expanded octahedron presented in section 5.2 are:

- Expanded octahedron ($p_{\text{folded}} = 2$) as a folded form of the double-expanded octahedron ($p_{\text{full}} = 3$)

$$\begin{pmatrix} \mathbf{e}^{\mathrm{I}} & \mathbf{e}^{\mathrm{II}} & \mathbf{e}^{\mathrm{III}} & \mathbf{e}^{\mathrm{IV}} \end{pmatrix} = \begin{pmatrix} \frac{7}{\sqrt{3}} & 7 & -7 & -1 \\ \frac{7}{\sqrt{3}} & 7 & -7 & -1 \\ -3\sqrt{3} & 3 & -3 & 11 \\ -3\sqrt{3} & 3 & -3 & 11 \\ 3\sqrt{3} & 3 & 73 & -1 \\ 3\sqrt{3} & 3 & 73 & -1 \\ -\frac{7}{\sqrt{3}} & -1 & 77 & 11 \\ -\frac{7}{\sqrt{3}} & -1 & 77 & 11 \\ 0 & 6 & 70 & -10 \\ 0 & 6 & 70 & -10 \\ \frac{8}{\sqrt{3}} & 2 & -2 & 14 \\ \frac{8}{\sqrt{3}} & 2 & -2 & 14 \\ -\frac{8}{\sqrt{3}} & 4 & 72 & -4 \\ -\frac{8}{\sqrt{3}} & 4 & 72 & -4 \\ 0 & 0 & 0 & 20 \\ 0 & 0 & 0 & 20 \\ -\frac{4}{\sqrt{3}} & 8 & -27 & -1 \\ -\frac{4}{\sqrt{3}} & 8 & -27 & -1 \\ 0 & 0 & 133 & -1 \\ 0 & 0 & 133 & -1 \\ 0 & 6 & -63 & 11 \\ 0 & 6 & -63 & 11 \\ \frac{4}{\sqrt{3}} & -2 & 97 & 11 \\ \frac{4}{\sqrt{3}} & -2 & 97 & 11 \end{pmatrix} \tag{32}$$

$$\alpha_s = \begin{pmatrix} \frac{-4c_{x_1}l_1 + 2c_{x_2}l_2 + c_{x_3}l_3}{28\sqrt{3}} & \frac{-4c_{y_1}l_1 + 2c_{y_2}l_2 + c_{y_3}l_3}{28\sqrt{3}} & \frac{-4c_{z_1}l_1 + 2c_{z_2}l_2 + c_{z_3}l_3}{28\sqrt{3}} \\ -\frac{39c_{x_1}l_1 + 37c_{x_2}l_2 - 36c_{x_3}l_3}{19648} & -\frac{39c_{y_1}l_1 + 37c_{y_2}l_2 - 36c_{y_3}l_3}{19648} & -\frac{39c_{z_1}l_1 + 37c_{z_2}l_2 - 36c_{z_3}l_3}{19648} \\ \frac{c_{x_1}l_1 + 18c_{x_2}l_2 + 40c_{x_3}l_3}{10640} & \frac{c_{y_1}l_1 + 18c_{y_2}l_2 + 40c_{y_3}l_3}{10640} & \frac{c_{z_1}l_1 + 18c_{z_2}l_2 + 40c_{z_3}l_3}{10640} \\ \frac{c_{x_1}l_1 + 2c_{x_2}l_2}{80} & \frac{c_{y_1}l_1 + 2c_{y_2}l_2}{80} & \frac{c_{z_1}l_1 + 2c_{z_2}l_2}{80} \end{pmatrix}$$

- X-expanded octahedron ($p_{\text{folded}} = 2$) as a folded form of the X-double-expanded octahedron ($p_{\text{full}} = 3$)

$$\begin{pmatrix} \mathbf{e}^{\mathrm{I}} & \mathbf{e}^{\mathrm{II}} & \mathbf{e}^{\mathrm{III}} & \mathbf{e}^{\mathrm{IV}} \end{pmatrix} = \begin{pmatrix} 13 & 13 & 13 & 1 \\ 13 & 13 & 13 & 1 \\ -14 & 7 & 7 & 19 \\ -14 & 7 & 7 & 19 \\ 14 & 7 & 253 & 1 \\ 14 & 7 & 253 & 1 \\ -13 & 1 & 247 & 19 \\ -13 & 1 & 247 & 19 \\ 0 & 14 & 260 & -20 \\ 0 & 14 & 260 & -20 \\ 9 & 2 & 2 & 34 \\ 9 & 2 & 2 & 34 \\ -9 & 12 & 258 & -14 \\ -9 & 12 & 258 & -14 \\ 0 & 0 & 0 & 40 \\ 0 & 0 & 0 & 40 \\ -3 & 18 & -187 & 1 \\ -3 & 18 & -187 & 1 \\ 0 & 0 & 533 & 1 \\ 0 & 0 & 533 & 1 \\ 0 & 14 & -273 & 19 \\ 0 & 14 & -273 & 19 \\ 3 & -4 & 447 & 19 \\ 3 & -4 & 447 & 19 \end{pmatrix} \tag{33}$$

$$\alpha_s = \begin{pmatrix} \frac{-9c_{x_1}l_1 + 3c_{x_2}l_2 + c_{x_3}l_3}{273} & \frac{-9c_{y_1}l_1 + 3c_{y_2}l_2 + c_{y_3}l_3}{273} & \frac{-9c_{z_1}l_1 + 3c_{z_2}l_2 + c_{z_3}l_3}{273} \\ \frac{5\left(c_{x_1}l_1 + 2c_{x_2}l_2 + 3c_{x_3}l_3\right)}{861} & \frac{5\left(c_{y_1}l_1 + 2c_{y_2}l_2 + 3c_{y_3}l_3\right)}{861} & \frac{5\left(c_{z_1}l_1 + 2c_{z_2}l_2 + 3c_{z_3}l_3\right)}{861} \\ \frac{-c_{x_1}l_1 - 43c_{x_2}l_2 + 120c_{x_3}l_3}{127920} & \frac{-c_{y_1}l_1 - 43c_{y_2}l_2 + 120c_{y_3}l_3}{127920} & \frac{-c_{z_1}l_1 - 43c_{z_2}l_2 + 120c_{z_3}l_3}{127920} \\ \frac{c_{x_1}l_1 + 3c_{x_2}l_2}{240} & \frac{c_{y_1}l_1 + 3c_{y_2}l_2}{240} & \frac{c_{z_1}l_1 + 3c_{z_2}l_2}{240} \end{pmatrix}$$

In Eqs. (29)–(33), $c_{x_1} = 1$, $c_{y_1} = c_{z_1} = 0$, $c_{x_2} = \cos\theta_{1-2}$, $c_{y_2} = \sin\theta_{1-2}$, $c_{z_2} = 0$, $c_{x_3} = \cos\theta_{1-3}$, $c_{y_3} = \frac{\cos\theta_{2-3} - \cos\theta_{1-2}\cos\theta_{1-3}}{\sin\theta_{1-2}} \in [-1, 1]$, and $c_{z_3} = \sqrt{\sin^2\theta_{1-3} - {c_{y_3}}^2}$.

References

[1] Zhang JY, Ohsaki M. Tensegrity structures: form, stability, and symmetry. Springer; 2015.

[2] Van Essen DC. Biomechanical models and mechanisms of cellular morphogenesis and cerebral cortical expansion and folding. Semin Cell Dev Biol 2023;140:90–104. https://doi.org/10.1016/j.semcdb.2022.06.007.

[3] Ingber DE. From tensegrity to human organs-on-chips: implications for mechanobiology and mechanotherapeutics. Biochem J 2023;480:243–57. https://doi.org/10.1042/BCJ20220303.

[4] Krivošej J, Beneš P, Zavřel J, Balon A, Halamka V, Šika Z. Energy efficient robots based on structures with tensegrity features and cable-driven mechanisms. Mech Mach Theory 2023;187:105364. https://doi.org/10.1016/J.MECHMACHTHEORY.2023.105364.

[5] Wang X, Ling Z, Qiu C, Song Z, Kang R. A four-prism tensegrity robot using a rolling gait for locomotion. Mech Mach Theory 2022;172:104828. https://doi.org/10.1016/j.mechmachtheory.2022.104828.

[6] Yue X-H, Yin X, Sun Z-Y, Liu L-Y, Wang Y, Xu G-K, et al. Flexible, lightweight, tunable robotic arms enabled by X-tensegrity inspired structures. Compos Struct 2024;344. https://doi.org/10.1016/j.compstruct.2024.118331.

[7] Shen Y, Chen M, Skelton RE. Markov data-based reference tracking control to tensegrity morphing airfoils. Eng Struct 2023;291:116430. https://doi.org/10.1016/j.engstruct.2023.116430.

[8] Wang X, Luo A, Liu H. Design and analysis of a double-helix tensegrity spherical lander. Mech Res Commun 2023;129:104091. https://doi.org/10.1016/j.mechrescom.2023.104091.

[9] Chen M, Goyal R, Majji M, Skelton RE. Design and analysis of a growable artificial gravity space habitat. Aerosp Sci Technol 2020;106. https://doi.org/10.1016/j.ast.2020.106147.

[10] Fraternali F, Santos F. Mechanical modeling of superelastic tensegrity braces for earthquake-proof structures. Extreme Mech Lett 2019;33:100578. https://doi.org/10.1016/j.eml.2019.100578.

[11] Shekastehband B, Ayoubi M. Nonlinear dynamic instability behavior of tensegrity grids subjected to impulsive loads. Thin-Walled Struct 2019;136:1–15. https://doi.org/10.1016/j.tws.2018.11.031.

[12] Flemons TE, Blostein D. New approaches to mechanizing tensegrity structures. In: Earth and Space 2018: Engineering for Extreme Environments - Proceedings of the 16th Biennial International Conference on Engineering, Science, Construction, and Operations in Challenging Environments; 2018, p. 910–22. https://doi.org/10.1061/9780784481899.086.

[13] Kumar S, Aswal N, Sen S. A novel Genetic algorithm based form-finding approach towards the improved design of tensegrity utility bridge. Structures 2023;58. https://doi.org/10.1016/j.istruc.2023.105401.

[14] Pajunen K, Johanns P, Pal RK, Rimoli JJ, Daraio C. Design and impact response of 3D-printable tensegrity-inspired structures. Mater Des 2019;182:107966. https://doi.org/10.1016/j.matdes.2019.107966.
[15] Yin X, Gao ZY, Zhang S, Zhang LY, Xu GK. Truncated regular octahedral tensegrity-based mechanical metamaterial with tunable and programmable Poisson's ratio. Int J Mech Sci 2020;167:105285. https://doi.org/10.1016/j.ijmecsci.2019.105285.
[16] Tan X, Wang B, Yao K, Zhu S, Chen S, Xu P, et al. Novel multi-stable mechanical metamaterials for trapping energy through shear deformation. Int J Mech Sci 2019;164:105168. https://doi.org/10.1016/J.IJMECSCI.2019.105168.
[17] Linkwitz K, Schek H-J. Einige Bemerkungen zur Berechnung von vorgespannten Seilnetzkonstruktionen. Ingenieur-Archiv 1971;40:145–58. https://doi.org/10.1007/BF00532146.
[18] Schek H-J. The force density method for form finding and computation of general networks. Comput Methods Appl Mech Eng 1974;3:115–34. https://doi.org/10.1016/0045-7825(74)90045-0.
[19] Hernández-Montes E, Jurado-Pia R, Bayo E. Topological mapping for tension structures. J Struct Eng 2006;132:970–7. https://doi.org/10.1061/(ASCE)0733-9445(2006)132:6(970).
[20] Carbonell-Márquez JF, Jurado-Piña R, Gil-Martín LM, Hernández-Montes E. Symmetry preserving in Topological Mapping for tension structures. Eng Struct 2013;52. https://doi.org/10.1016/j.engstruct.2013.02.011.
[21] Sánchez J, Serna MÁ, Morer P. A multi-step force–density method and surface-fitting approach for the preliminary shape design of tensile structures. Eng Struct 2007;29:1966–76. https://doi.org/10.1016/j.engstruct.2006.10.015.
[22] Liew A. Constrained Force Density Method optimisation for compression-only shell structures. Structures 2020;28:1845–56. https://doi.org/10.1016/j.istruc.2020.09.078.
[23] Carbonell-Márquez JF, Gil-Martín LM, Fernández-Ruíz MA, Hernández-Montes E. Topological design of compression structures. Arch Appl Mech 2016;86:1495–508. https://doi.org/10.1007/s00419-016-1131-y.
[24] Fernández-Ruiz MA, Hernández-Montes E, Carbonell-Márquez JF, Gil-Martín LM. Patterns of force: length ratios for the design of compression structures with inner ribs. Eng Struct 2017;148:878–89. https://doi.org/10.1016/j.engstruct.2017.07.027.
[25] Moskaleva A, Gusev S, Konev S, Sergeichev I, Safonov A, Hernandez-Montes E. Composite freeform shell structures: design, construction and testing. Compos Struct 2023;306:116603. https://doi.org/10.1016/J.COMPSTRUCT.2022.116603.
[26] Tran HC, Lee J. Advanced form-finding of tensegrity structures. Comput Struct 2010;88:237–46. https://doi.org/10.1016/j.compstruc.2009.10.006.
[27] Nagase K, Yamashita T, Kawabata N. On a connectivity matrix formula for tensegrity prism plates. Mech Res Commun 2016;77:29–43. https://doi.org/10.1016/j.mechrescom.2016.08.003.
[28] Sonawane A, Hawaldar C, Ankad P, Joshi A. Non-linear geometric analysis of multilayer tensegrity tower. Mater Today Proc 2023;77:788–93. https://doi.org/10.1016/j.matpr.2022.11.448.
[29] Jiang J-H, Yin X, Xu G-K, Wang Z-Y, Zhang L-Y. A unified analytical form-finding of truncated regular octahedral tensegrities. Int J Mech Sci 2023;239:107857. https://doi.org/10.1016/j.ijmecsci.2022.107857.
[30] Lee S, Lee J. A novel method for topology design of tensegrity structures. Compos Struct 2016;152:11–9. https://doi.org/10.1016/J.COMPSTRUCT.2016.05.009.
[31] Zhang L-Y, Jiang J-H, Wei K, Yin X, Xu G-K, Zhang J. Self-equilibrium and super-stability of rhombic truncated regular tetrahedral and cubic tensegrities using symmetry-adapted force-density matrix method. Int J Solids Struct 2021;233:111215. https://doi.org/10.1016/j.ijsolstr.2021.111215.
[32] Song K, Scarpa F, Schenk M. Form-finding of tessellated tensegrity structures. Eng Struct 2022;252:113627. https://doi.org/10.1016/j.engstruct.2021.113627.
[33] Xu X, Huang S, Shu T, Wang Y, Luo Y. A novel two-step tensegrity topology-finding method based on mixed integer programming and nonlinear programming. Int J Steel Struct 2022;22:1266–82. https://doi.org/10.1007/s13296-022-00634-x.
[34] Fernández-Ruiz MA, Hernández-Montes E, Gil-Martín LM. Topological design of the octahedron tensegrity family. Eng Struct 2022;259:114211. https://doi.org/10.1016/j.engstruct.2022.114211.
[35] Fernández-Ruiz MA, Hernández-Montes E, Gil-Martín LM. The Z-octahedron family: a new tensegrity family. Eng Struct 2020;222:111151. https://doi.org/10.1016/j.engstruct.2020.111151.
[36] Fernández-Ruiz MA, Hernández-Montes E, Gil-Martín LM. The Octahedron family as a source of tensegrity families: The X-Octahedron family. Int J Solids Struct 2021;208–209:1–12. https://doi.org/10.1016/j.ijsolstr.2020.10.019.
[37] Fernández-Ruiz MA, Hernández-Montes E, Carbonell-Márquez JF, Gil-Martín LM. Octahedron family: the double-expanded octahedron tensegrity. Int J Solids Struct 2019;165:1–13. https://doi.org/10.1016/j.ijsolstr.2019.01.017.
[38] Connelly R. Tensegrity structures: why are they stable? In: Thorpe M, Duxbury P, editors. Rigidity theory and applications. Fundamental material research. Boston, MA: Springer; 1999. p. 47–54. https://doi.org/10.1007/0-306-47089-6_3.
[39] Zhang JY, Ohsaki M. Stability conditions for tensegrity structures. Int J Solids Struct 2007;44:3875–86. https://doi.org/10.1016/j.ijsolstr.2006.10.027.
[40] Hernández L, Fernández-Ruiz MA, Gil-Martín LM. Influence of the level of connectivity on the members of the Octahedron and X-Octahedron families of tensegrities. Eng Stuct 2023;1–2. https://doi.org/10.1016/j.engstruct.2023.116927.
[41] Hernández-Montes E, Fernández-Ruiz MA, Gil-Martín LM, Merino L, Jara P. Full and folded forms: a compact review of the formulation of tensegrity structures. Math Mech Solids 2018;23:944–9. https://doi.org/10.1177/1081286517697372.
[42] Heping L, Jian S, Yupeng Q, Ani L. Analysis for a novel folding frame tensegrity tent. Structures 2023;57:105085. https://doi.org/10.1016/j.istruc.2023.105085.
[43] Rhode-Barbarigos L, Hadj Ali NB, Motro R, Smith IFC. Designing tensegrity modules for pedestrian bridges. Eng Struct 2010;32:1158–67. https://doi.org/10.1016/j.engstruct.2009.12.042.